Reconfigurable Electromagnetic Environments: A General Framework

Davide Dardari, *Senior Member, IEEE*

***Abstract*— The recent introduction of the smart radio environments (SREs) paradigm, facilitated by reconfigurable intelligent surfaces (RISs) and large surface antennas, has highlighted the need for physically consistent models and design tools in communication systems that integrate information theory (IT) and electromagnetic (EM) theory. In this paper, we present a comprehensive framework for characterizing and designing programmable EM environments, based on rigorous EM arguments and represented through a linear graph employing matrix operators. The framework enables the determination of the EM transfer function of the system and the channel matrix used in IT, along with their relationship as functions of the programmable parameters. Considering that the mapping of EM quantities into IT signals occurs through the presence of ports in antenna structures, using the framework, we analyze the constraints imposed by the ports in terms of potential degrees-of-freedom (DoF) and establish the fundamental limits on the DoF of large surface antennas. To demonstrate the utility and validity of the framework, we provide examples specifically related to the characterization and optimization of RISs.**

***Index Terms*— Smart radio environments, holographic MIMO, EM transfer function, reconfigurable intelligent surfaces, antenna degrees of freedom.**

I. Introduction

RECENTLY, the concept of smart radio environments (SREs) has emerged as one of the new design paradigms for next-generation networks [1]. With the deployment of programmable electromagnetic (EM) devices, such as reconfigurable intelligent surfaces (RISs), in SREs, the environment becomes an integral part of the design and optimization process. This advancement is expected to lead to more flexible wireless networks, offering improved performance in terms of achievable data rates, interference shaping, coverage extension, energy efficiency, and complexity reduction.

Extensive research has been dedicated to the study of communication and localization systems aided by RISs, as evident from the papers [2], [3], [4], [5]. Simultaneously, the introduction of extremely electrically large antennas, often denoted to as large intelligent surfaces (LISs), constructed using metasurfaces and designed to operate at high frequencies (millimeter waves and THz), has enabled the utilization of radiating near-field characteristics of the radio channel, even at practical distances [2], [6], [7], [8], [9]. For example, at 100 GHz, the near-field region of an antenna with an aperture of 50 cm extends up to 100 m [2].

Despite the wide range of literature available today on the subject, previous studies have some main shortcomings that can be summarized as follows. On the one hand, system-level design and optimization have often relied on oversimplified but tractable models, which unfortunately incorporate physically inconsistent assumptions. These models fail to capture important peculiarities of the electromagnetic objects (EMOs) that form the system, such as antennas, RISs, passive scatterers, and more. One typical example of an often neglected EM phenomenon exhibited in smart metasurfaces is the presence of Floquet modes. These modes are the effect of the periodic impedance of a metasurface and can lead to spurious reflections, potentially causing interference at undesired angles and compromising the overall system performance [10]. Moreover, the pursuit of ultimate theoretical limits requires an accurate description of the underlying EM phenomena [11], [12], as well as understanding their relationship with the models commonly adopted in information theory (IT). On the other hand, in the EM community, the emphasis has primarily been on characterizing individual devices, often relying on extensive EM-level simulations. However, these simulations are challenging to incorporate into a system-level analysis or real-time system optimization cycle [10], [13], [14], [15], [16], [17]. In the past, this dichotomy has been reasonable, as the EMOs, such as antennas, were perceived as mere "sensors" or "actuators/transducers" within the IT community. However, in the near future, with the presence of reconfigurable EM environments, the primary objective will be to optimize the system response, even in real-time, by adjusting the parameters of the EMOs (e.g., the reflection properties of a metasurface-based RIS). This necessitates a holistic system view that incorporates physically consistent models and design tools, seamlessly integrating IT and EM theory [18]. Some recent works have taken steps in this direction. The investigation of the DoF of the wireless channel when using LISs has been conducted in [6], [7], [12], and [2]. These works model the surface as a continuum of infinitesimal antenna elements. As for RISs, the work in [19] proposes modeling a RIS as a set of elementary coupled dipoles and characterizing its response in terms of impedance matrices. In [20], both continuous and discrete models for the response of a perfect reflecting RIS are derived based on EM arguments. However, it is worth

Manuscript received 1 April 2023; revised 21 November 2023; accepted 28 November 2023. Date of publication 15 April 2024; date of current version 29 May 2024. This work was supported by European Union (EU) under Italian National Recovery and Resilience Plan (NRRP) of NextGenerationEU, partnership on "Telecommunications of the Future" (Program RESTART) under Grant PE00000001 - Spoke 7.

The author is with Dipartimento di Ingegneria dell'Energia Elettrica e dell'Informazione "Guglielmo Marconi" (DEI), WiLAB-CNIT, University of Bologna, Cesena Campus, I-47521 Cesena, Italy (e-mail: davide.dardari@unibo.it).

Color versions of one or more figures in this article are available at https://doi.org/10.1109/JSAC.2024.3389117.

Digital Object Identifier 10.1109/JSAC.2024.3389117

noting that most discrete-element models are not suitable for describing all the phenomena (e.g., Floquet modes) that characterize homogeneous metamaterial-based RIS imposing EM boundary conditions. A recent investigation on the connections and discrepancies between continuous and discrete models has been published in [21]. For a comprehensive survey that includes a critical discussion on RIS modeling, the reader can refer to [22].

Moving to a system level, the authors in [23] introduce the concept of the *EM transfer function* in the wavenumber domain, similar to the classical transfer function used in the signal processing community for linear systems in the frequency domain. This concept has been further developed in recent papers [3], [24], [25], [26]. In particular, [24] and [25] extend the concept of EM transfer function to a stochastic Gaussian propagation environment with rich scattering. The paper [26] derives the EM transfer function for the case of an infinite-sized surface with a constant reflection coefficient by establishing a connection between the well-known image theorem in EM theory and the EM transfer function. Furthermore, [27] presents a generalized expression of the EM field reflected by an EM skin in far-field and radiative near-field regimes, which is subsequently utilized to derive a unified method for designing anomalous-reflecting and focusing EM skins.

The previously mentioned studies are limited to defining the EM transfer function as a "black box", offering no general methodology to compute it, except for a few oversimplified scenarios or undersimplified assumptions (e.g., neglecting polarization, assuming infinite uniform surfaces, point-wise scatterers, and far-field regime). None of these papers address the characterization of the EM transfer function for general reconfigurable EMOs like RISs and LISs. Furthermore, the relationship between the EM transfer function and the channel matrix concept, which is typical in IT, has not been thoroughly investigated. For instance, most of the literature mentioned above assumes that LIS antennas can realize any current distribution on their surface. On the other hand, the signals considered in IT models are associated with electrical quantities defined at the antenna ports, and the antenna structure imposes a limitation on the actual DoF of the antenna in generating the current distribution.

To address this gap, this paper introduces a comprehensive framework rooted in rigorous EM arguments, applicable in both far-field and near-field regimes (radiative and reactive). The aim is to offer an IT and physically consistent interpretation of reconfigurable EM environments. The primary contributions and the organization of this paper are summarized as follows:

- The problem formulation for describing a reconfigurable EM system, incorporating multiple EMOs based on a vector representation of fields to capture the underlying EM phenomena, reveals that any system with linear EMOs can be represented as a space-variant feedback system.
- Acknowledging the inherent complexity of analyzing and designing space-variant feedback systems, this paper proposes a linear algebra description of the EM system (Sec. III). This involves introducing harmonic basis functions (referred to as *modes*) (Sec. IV) and subsequently deriving expressions for mode coupling (Sec. V). This approach provides a graph-based interpretation of the system, beneficial for designing and characterizing EM systems, even when reconfigurable EMOs are involved.
- The modeling and characterization of reconfigurable surfaces in terms of boundary conditions are discussed in Sec. VI. It is demonstrated that classical local boundary conditions limit the structure of the surface's transfer function, whereas utilizing global boundary conditions provides the highest level of flexibility.
- In Sec. VII, we demonstrate that the graph-based interpretation of the system, coupled with the linear algebra representation, successfully establishes the relationship between the EM transfer function and the IT channel matrix by considering the constraints imposed by the presence of ports in antenna structures. This representation acts as a "bridge" between the two worlds.
- We further analyze the constraints imposed by the antenna's ports in terms of potential DoF. To this end, a general approach to evaluate the impedance matrix of antenna structures is presented and subsequently utilized to determine the theoretical upper bound on the DoF of any antenna structure as a function of its shape (Sec. VII-B). To illustrate the utility of the proposed framework, three examples are provided in Sec. VIII: *(i)* Derivation of the EM transfer function of a finite-size surface with a given impedance, demonstrating that previous results in the literature can be viewed as particular cases of our work; *(ii)* Design of a RIS aiming to minimize spurious interference caused by the presence of Floquet modes and/or other EM sources. A comparison is made between the design using local and global boundary conditions; *(iii)* Derivation of a closed-form expression for the impedance matrix of a LIS antenna and its theoretical DoF, compared with spherical and discrete-element antennas.

A. Notation and Definitions

Lowercase bold variables denote vectors in the 3D space, i.e., $\mathbf{r} = r_x\,\hat{\mathbf{x}} + r_y\,\hat{\mathbf{y}} + r_z\,\hat{\mathbf{z}}$ is a vector with Cartesian coordinates (r_x, r_y, r_z), $\hat{\mathbf{r}}$ is a unit vector denoting its direction, and $r = |\mathbf{r}|$ denotes its magnitude, where $\hat{\mathbf{x}}$, $\hat{\mathbf{y}}$, and $\hat{\mathbf{z}}$ represent the unit vectors in the x, y and z directions, respectively. The cross product between vectors $\mathbf{p}$ and $\mathbf{r}$ is indicated with $\mathbf{p} \times \mathbf{r}$, whereas the scalar product with $\mathbf{p} \cdot \mathbf{r}$. $\delta(x)$ and δ_n represent, respectively, the Dirac delta pseudo-function and its discrete counterpart (Kronecker delta). Multi-variable versions can be defined as well, i.e., $\delta(\mathbf{r}) = \delta(x)\,\delta(y)\,\delta(z)$ and $\delta_{n,m} = \delta_{n-m}$. Sans serif capital letters (e.g., $\mathsf{E}(\mathbf{r})$, $\mathsf{J}(\mathbf{r})$) represent EM vector functions (in the following named *fields*), whereas scalar functions are denoted with lowercase letters, i.e., $\phi(\mathbf{r})$. Boldface capital letters are matrices (e.g., $\mathbf{A}$), where $\mathbf{I}_N$ and $\mathbf{0}_N$ are, respectively, the identity and zero matrices of size N, $a_{n,m} = [\mathbf{A}]_{n,m}$ represents the (n,m)th element of matrix $\mathbf{A}$, * indicates the complex conjugate operator, whereas $\mathbf{A}^{\mathrm{H}}$ the conjugate transpose of $\mathbf{A}$. $\nabla \times \mathsf{E}(\mathbf{r})$ is the curl of the vector function $\mathsf{E}(\mathbf{r})$. Surfaces and volumes are indicated with calligraphic letters $\mathcal{S}$. Any linear transformation of a field $\mathsf{A}(\mathbf{r})$ into a field $\mathsf{B}(\mathbf{r})$ can be described using

a 2-rank tensor matrix that can be expressed according to vector notation $\mathsf{B}(\mathbf{r}) = \underline{\mathsf{D}} \cdot \mathsf{A}(\mathbf{r})$ and algebra, where $\underline{\mathsf{D}}$ is called *dyadic*. Typically, $\underline{\mathsf{D}}$ depends on the position $\mathbf{r}$ even though this is not shown explicitly to lighten the notation. Often an operation involving a dyadic can be expressed in matrix form. Define $\mathrm{Sinc}(x) = \sin(\pi x)/(\pi x)$ for $x \neq 0$, 1 for $x = 0$, and $\mathrm{Rect}(x) = 1$ for $|x| < 1/2$, zero otherwise. Furthermore, denote with μ, ϵ, and $\eta = \sqrt{\mu/\epsilon}$ the free-space permittivity, permeability, and impedance, respectively, and c the speed of light. Finally, we define $\mathbb{E}\{x\}$ the statistical expectation of the random variable x and $\mathbf{n} \sim \mathcal{N}_c(\mathbf{m}, \mathbf{C})$ a complex-valued Gaussian random vector with mean $\mathbf{m}$ and covariance matrix $\mathbf{C}$.

II. Reconfigurable EM System

A. Problem Formulation

We consider M linear time-invariant EMOs are present in the system sketched in Fig. 1, and we indicate with $\mathcal{S}^{(m)}$, $m = 1, 2, \ldots, M$, the surface that encloses the mth EMO. Each surface can represent the physical surface of the EMO or any arbitrary surface that encloses it. An EMO may identify a RIS, a conventional transmitting/receiving antenna, a reconfigurable antenna, such as a dynamic metasurface antenna [28], and any other object in the environment affecting the propagation conditions. We work in the frequency domain, where time-harmonic excitations are assumed with angular frequency ω, but not shown explicitly. Denote with $\mathsf{J}^{(m)}(\mathbf{r})$ and $\mathsf{M}^{(m)}(\mathbf{r})$ the electric and magnetic current densities, respectively, on surface $\mathcal{S}^{(m)}$. Notice that $\mathsf{J}^{(m)}(\mathbf{r})$ and $\mathsf{M}^{(m)}(\mathbf{r})$ are zero outside $\mathcal{S}^{(m)}$. The total electric and magnetic currents present in the system are given by $\mathsf{J}(\mathbf{r}) = \sum_{m=1}^{M} \mathsf{J}^{(m)}(\mathbf{r})$ and $\mathsf{M}(\mathbf{r}) = \sum_{m=1}^{M} \mathsf{M}^{(m)}(\mathbf{r})$, respectively. In general, $\mathsf{J}^{(m)}(\mathbf{r})$ and $\mathsf{M}^{(m)}(\mathbf{r})$ can be decomposed into the sum of the (real or equivalent) impressed $\left(\mathsf{J}_{\mathrm{imp}}^{(m)}(\mathbf{r}), \mathsf{M}_{\mathrm{imp}}^{(m)}(\mathbf{r})\right)$ (if any) and induced $\left(\mathsf{J}_{\mathrm{s}}^{(m)}(\mathbf{r}), \mathsf{M}_{\mathrm{s}}^{(m)}(\mathbf{r})\right)$ currents, that is, $\mathsf{J}^{(m)}(\mathbf{r}) = \mathsf{J}_{\mathrm{s}}^{(m)}(\mathbf{r}) + \mathsf{J}_{\mathrm{imp}}^{(m)}(\mathbf{r})$ and $\mathsf{M}^{(m)}(\mathbf{r}) = \mathsf{M}_{\mathrm{s}}^{(m)}(\mathbf{r}) + \mathsf{M}_{\mathrm{imp}}^{(m)}(\mathbf{r})$. According to the equivalent principle [29, Ch. 12], the introduction of (fictitious) induced currents, satisfying the boundary conditions at the corresponding surface, permits to consider the induced current sources to radiate into an unbounded space. Therefore, the EM field, i.e., the electric and magnetic fields, generated by all the currents present in the system at the generic location $\mathbf{r}$ can be computed under the free-space condition, that is,

$$\begin{pmatrix} \mathsf{E}(\mathbf{r}) \\ \mathsf{H}(\mathbf{r}) \end{pmatrix} = \begin{pmatrix} \underline{\mathsf{G}}_{\mathrm{EJ}} & \underline{\mathsf{G}}_{\mathrm{EM}} \\ \underline{\mathsf{G}}_{\mathrm{HJ}} & \underline{\mathsf{G}}_{\mathrm{HM}} \end{pmatrix} \cdot \begin{pmatrix} \mathsf{J}(\mathbf{r}) \\ \mathsf{M}(\mathbf{r}) \end{pmatrix} = \underline{\mathsf{G}} \cdot \begin{pmatrix} \mathsf{J}(\mathbf{r}) \\ \mathsf{M}(\mathbf{r}) \end{pmatrix} \tag{1}$$

where the above dyadics are given by [30, Ch. 3]

$$\underline{\mathsf{G}}_{\mathrm{EJ}} \cdot \mathsf{J}(\mathbf{r}) = \frac{1}{j\omega\epsilon} \nabla_{\mathrm{x}} \nabla_{\mathrm{x}} \int_{\mathcal{S}} G_0(\mathbf{r} - \mathbf{s})\, \mathsf{J}(\mathbf{s})\, d\mathbf{s} \tag{2}$$

$$\underline{\mathsf{G}}_{\mathrm{EM}} \cdot \mathsf{M}(\mathbf{r}) = -\nabla_{\mathrm{x}} \int_{\mathcal{S}} G_0(\mathbf{r} - \mathbf{s})\, \mathsf{M}(\mathbf{s})\, d\mathbf{s} \tag{3}$$

$$\underline{\mathsf{G}}_{\mathrm{HJ}} \cdot \mathsf{J}(\mathbf{r}) = \nabla_{\mathrm{x}} \int_{\mathcal{S}} G_0(\mathbf{r} - \mathbf{s})\, \mathsf{J}(\mathbf{s})\, d\mathbf{s} \tag{4}$$

$$\underline{\mathsf{G}}_{\mathrm{HM}} \cdot \mathsf{M}(\mathbf{r}) = \frac{1}{j\omega\mu} \nabla_{\mathrm{x}} \nabla_{\mathrm{x}} \int_{\mathcal{S}} G_0(\mathbf{r} - \mathbf{s})\, \mathsf{M}(\mathbf{s})\, d\mathbf{s} \tag{5}$$

being $\mathcal{S} = \bigcup_{m=1}^{M} \mathcal{S}^{(m)}$. The function

$$G_0(\mathbf{r}) = \frac{\exp(-jk_0|\mathbf{r}|)}{4\pi|\mathbf{r}|} \tag{6}$$

is the free-space scalar Green's function, where $k_0 = 2\pi/\lambda$ is the wavenumber and $\lambda = 2\pi c/\omega$ is the wavelength. It can be easily noticed from the previous equations that the propagation phenomenon operates as a space-invariant linear filter because $G_0(\mathbf{r})$ appears in (2)-(5) as a function of only the difference $\mathbf{r} - \mathbf{s}$.

Define the EM field $\left(\mathsf{E}_{\mathrm{t}}^{(m)}(\mathbf{r}), \mathsf{H}_{\mathrm{t}}^{(m)}(\mathbf{r})\right)$ tangent to surface $\mathcal{S}^{(m)}$ of the mth EMO. For any linear time-invariant EMO, the induced currents are linear functionals of the EM field tangent to the surface so that they can be described as follows (*constitutive equation*) [7]

$$\begin{aligned} \begin{pmatrix} \mathsf{J}_{\mathrm{s}}^{(m)}(\mathbf{r}) \\ \mathsf{M}_{\mathrm{s}}^{(m)}(\mathbf{r}) \end{pmatrix} &= \begin{pmatrix} \underline{\mathsf{D}}_{\mathrm{JE}}^{(m)} & \underline{\mathsf{D}}_{\mathrm{JH}}^{(m)} \\ \underline{\mathsf{D}}_{\mathrm{ME}}^{(m)} & \underline{\mathsf{D}}_{\mathrm{MH}}^{(m)} \end{pmatrix} \cdot \begin{pmatrix} \mathsf{E}_{\mathrm{t}}^{(m)}(\mathbf{r}) \\ \mathsf{H}_{\mathrm{t}}^{(m)}(\mathbf{r}) \end{pmatrix} \\ &= \underline{\mathsf{D}}^{(m)} \cdot \begin{pmatrix} \mathsf{E}_{\mathrm{t}}^{(m)}(\mathbf{r}) \\ \mathsf{H}_{\mathrm{t}}^{(m)}(\mathbf{r}) \end{pmatrix} \end{aligned} \tag{7}$$

where the dyadic $\underline{\mathsf{D}}_{\mathrm{JE}}^{(m)}$ can be expressed in general as

$$\underline{\mathsf{D}}_{\mathrm{JE}}^{(m)} \cdot \mathsf{E}_{\mathrm{t}}^{(m)}(\mathbf{r}) = \int_{\mathcal{S}^{(m)}} \underline{\mathsf{D}}_{\mathrm{JE}}^{(m)}(\mathbf{r}, \mathbf{s})\, \mathsf{E}_{\mathrm{t}}^{(m)}(\mathbf{s})\, d\mathbf{s} \tag{8}$$

being $\underline{\mathsf{D}}_{\mathrm{JE}}^{(m)}(\mathbf{r}, \mathbf{s})$ the impulse response dyadic describing completely the relationship between the electric field and the induced current at the mth EMO. Similar expressions can be written for the dyadics $\underline{\mathsf{D}}_{\mathrm{JH}}^{(m)}$, $\underline{\mathsf{D}}_{\mathrm{ME}}^{(m)}$, and $\underline{\mathsf{D}}_{\mathrm{MH}}^{(m)}$. For instance, in non-magnetic scatterers, the induced magnetic current is zero, i.e., $\mathsf{M}_{\mathrm{s}}^{(m)}(\mathbf{r}) = 0$, then $\underline{\mathsf{D}}_{\mathrm{ME}}^{(m)} = \underline{\mathsf{D}}_{\mathrm{MH}}^{(m)} = 0$ [31]. The particular form of $\underline{\mathsf{D}}^{(m)}$ depends on the model adopted for the EMO and the target level of accuracy. Some examples are provided in Sec. VI. Looking at the relationship between (1) and (7), it is interesting to highlight that any EM scenario can be viewed as a feedback system of which it might of interest defining the EM transfer function (see Sec. II-D), and in which the impressed currents represent the inputs, the propagation phenomenon $\underline{\mathsf{G}}$ is a space-invariant filter and each EMO can be seen as a space-variant filter (in analogy with time-variant filters) whose output consists of the induced currents. The above feedback system involves integral equations whose solution is, in general, a complex problem typically addressed numerically. In this paper, we introduce a methodology to bypass this problem.

B. Antennas as EMOs With Input and Output Ports

In any practical communication system, the EM field is altered in response to electrical signals carrying information. The system also "senses" the EM field at various locations to retrieve this information by processing the electrical signals obtained from it. Radiating systems (antennas) play a crucial role in establishing the mapping between the EM field and IT signals through their input and output ports at which voltages (currents) are associated with input and output signals in the IT sense, respectively. To elaborate, consider a generic EMO representing a transmitting antenna equipped with P input

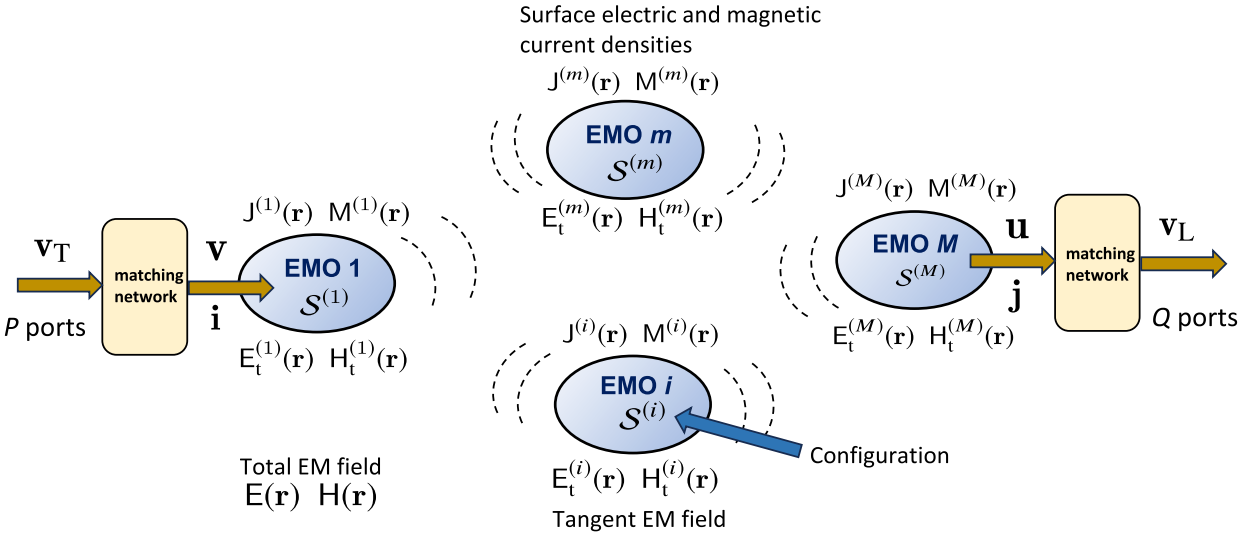

Fig. 1. General EM scenario with interacting EMOs. As an example, EMOs 1 and M represent a transmitting antenna with P input ports and a receiving antenna with Q output ports, respectively. The ith EMO can be configured (e.g., RIS).

ports (see Fig. 1). Signals are associated with the voltage envelopes $\mathbf{v} = [v_1, v_2, \ldots, v_P]^T$ at the P ports that are assumed to be properly matched to the corresponding impedance. Let $\mathbf{i} = [i_1, i_2, \ldots, i_P]^T$ denote the current envelopes flowing into the ports. Since they carry information, they must be considered as random variables. For notation convenience, we have omitted the explicit time index. The relationship between these voltage and current envelopes is given by the impedance matrix $\mathbf{Z}_{\mathrm{T}}$, which quantifies the mutual coupling within the antenna, such that $\mathbf{v} = \mathbf{Z}_{\mathrm{T}} \cdot \mathbf{i}$. In general, according to the equivalent principle, the radiating structure can be replaced by an equivalent impressed current density $\mathsf{J}_{\mathrm{imp}}(\mathbf{r})$ radiating in free space, which is linearly dependent on the currents $\mathbf{i}$. That is, $\mathsf{J}_{\mathrm{imp}}(\mathbf{r}) = \mathsf{T}(\mathbf{r}; \mathbf{i})$, where the mapping function $\mathsf{T}(\cdot)$ clearly depends on the antenna structure and material. We assume that the coupling with nearby objects (within the reactive field of the antenna) is already accounted for by $\mathsf{T}(\cdot)$, allowing us to set $\underline{\mathsf{D}} \simeq 0$, and assume $\mathsf{T}(\cdot)$ does not depend on the rest of the system. From a practical standpoint, $\mathsf{T}(\mathbf{r}; \mathbf{i})$ can be derived once the electrical field $\mathsf{E}(\mathbf{r})$ is known in the far field, and by inverting (14) with $\mathsf{M}(\mathbf{r}) = 0$ and $\mathsf{J}(\mathbf{r}) = \mathsf{J}_{\mathrm{imp}}(\mathbf{r})$. This can be achieved through measurements of the radiation pattern, analytical methods, or EM numerical simulations. By invoking the reciprocity theorem, similar considerations can be drawn for an EMO representing a receiving antenna with Q ports and impedance matrix $\mathbf{Z}_{\mathrm{R}}$, where $\mathbf{u} = \mathbf{Z}_{\mathrm{R}} \cdot \mathbf{j}$, and $\mathbf{u}$ and $\mathbf{j}$ are the voltage and current vectors at the output of the antenna, respectively, assumed to be perfectly matched. We will see in Sec. VII-B that the impedance matrix determines the DoF of the antenna in generating the impressed current $\mathsf{J}_{\mathrm{imp}}(\mathbf{r})$. Therefore, in the same section, a general method to derive it will be proposed and used to find the theoretical limits of a surface antenna.

C. Wavenumber Domain Representation

For what follows, it is convenient to introduce the representation of the fields in the wavenumber domain $\boldsymbol{\kappa} = \kappa_x \hat{\mathbf{x}} + \kappa_y \hat{\mathbf{y}} + \kappa_z \hat{\mathbf{z}}$ through the 3D Fourier transform. Specifically, given a generic field $\mathsf{A}(\mathbf{r})$, we can write

$$\widetilde{\mathsf{A}}(\boldsymbol{\kappa}) = \mathcal{F}\left[\mathsf{A}(\mathbf{r})\right] = \int_{\mathcal{R}^3} \mathsf{A}(\mathbf{r})\, e^{-\jmath \boldsymbol{\kappa}\cdot\mathbf{r}}\, d\mathbf{r} \tag{9}$$

$$\mathsf{A}(\mathbf{r}) = \mathcal{F}^{-1}\left[\widetilde{\mathsf{A}}(\boldsymbol{\kappa})\right] = \frac{1}{(2\pi)^3} \int_{\mathcal{R}^3} \widetilde{\mathsf{A}}(\boldsymbol{\kappa})\, e^{\jmath \boldsymbol{\kappa}\cdot\mathbf{r}}\, d\boldsymbol{\kappa}\,. \tag{10}$$

When applied to the EM field, the inverse Fourier representation in (10) expresses the EM field in terms of mathematical plane waves [32]. By inspection of (10), the plane wave with wavenumber $\boldsymbol{\kappa}$, travels in the positive w-direction (forward wave), with $w \in \{x, y, z\}$, when its component $\boldsymbol{\kappa}_w < 0$, whereas when $\boldsymbol{\kappa}_w > 0$ the wave travels in the negative w-direction (backward wave). By applying the Fourier transform to the Green's function (6) we obtain

$$\widetilde{G}_0(\boldsymbol{\kappa}) = \mathcal{F}\left[G_0(\mathbf{r})\right] = \frac{1}{|\boldsymbol{\kappa}|^2 - k_0^2} \tag{11}$$

and, from (2)-(5), that

$$\begin{aligned}\widetilde{\mathsf{E}}(\boldsymbol{\kappa}) = \mathcal{F}\left[\mathsf{E}(\mathbf{r})\right] &= \frac{\jmath\, \widetilde{G}_0(\boldsymbol{\kappa})}{\omega\epsilon} \boldsymbol{\kappa} \times \boldsymbol{\kappa} \times \widetilde{\mathsf{J}}(\boldsymbol{\kappa}) - \jmath\, \widetilde{G}_0(\boldsymbol{\kappa})\, \boldsymbol{\kappa} \times \widetilde{\mathsf{M}}(\boldsymbol{\kappa}) \\ &= \jmath\, \widetilde{G}_0(\boldsymbol{\kappa}) \boldsymbol{\kappa} \times \left[\frac{\eta}{k_0} \boldsymbol{\kappa} \times \widetilde{\mathsf{J}}(\boldsymbol{\kappa}) - \widetilde{\mathsf{M}}(\boldsymbol{\kappa})\right] \end{aligned} \tag{12}$$

$$\begin{aligned}\widetilde{\mathsf{H}}(\boldsymbol{\kappa}) = \mathcal{F}\left[\mathsf{H}(\mathbf{r})\right] &= \frac{\jmath\, \widetilde{G}_0(\boldsymbol{\kappa})}{\omega\mu} \boldsymbol{\kappa} \times \boldsymbol{\kappa} \times \widetilde{\mathsf{M}}(\boldsymbol{\kappa}) + \jmath\, \widetilde{G}_0(\boldsymbol{\kappa})\, \boldsymbol{\kappa} \times \widetilde{\mathsf{J}}(\boldsymbol{\kappa}) \\ &= \jmath\, \widetilde{G}_0(\boldsymbol{\kappa})\, \boldsymbol{\kappa} \times \left[\frac{1}{k_0\, \eta} \boldsymbol{\kappa} \times \widetilde{\mathsf{M}}(\boldsymbol{\kappa}) + \widetilde{\mathsf{J}}(\boldsymbol{\kappa})\right] \end{aligned} \tag{13}$$

where convolutions become multiplications in the wavenumber domain, $\widetilde{\mathsf{J}}(\boldsymbol{\kappa}) = \mathcal{F}\left[\mathsf{J}(\mathbf{r})\right]$, $\widetilde{\mathsf{M}}(\boldsymbol{\kappa}) = \mathcal{F}\left[\mathsf{M}(\mathbf{r})\right]$, and we have considered that $\mathcal{F}\left[\nabla \times \mathsf{A}\right] = \jmath\, \boldsymbol{\kappa} \times \widetilde{\mathsf{A}}(\boldsymbol{\kappa})$. The spatial filtering operated by the Green's operator is evident in (11) which corresponds to a low-pass filter with a cut-off frequency equal to k_0. This means that the EM field has a spatial low-pass characteristic. Incidentally, by defining $\boldsymbol{\kappa}_{\mathbf{r}} = k_0\, \hat{\mathbf{r}}$, the EM field at location $\mathbf{r}$ in far-field conditions is proportional to the

Fourier transform of the sources [29, Ch. 12], that is,

$$\mathsf{E}(\mathbf{r}) \simeq \jmath k_0 \frac{e^{-\jmath k_0 |\mathbf{r}|}}{4\pi|\mathbf{r}|} \hat{\mathbf{r}} \times \left[\eta\, \hat{\mathbf{r}} \times \widetilde{\mathsf{J}}(\boldsymbol{\kappa}_\mathbf{r}) + \widetilde{\mathsf{M}}(\boldsymbol{\kappa}_\mathbf{r})\right]$$
$$\mathsf{H}(\mathbf{r}) \simeq \jmath k_0 \frac{e^{-\jmath k_0 |\mathbf{r}|}}{4\pi|\mathbf{r}|} \hat{\mathbf{r}} \times \left[\frac{1}{\eta}\, \hat{\mathbf{r}} \times \widetilde{\mathsf{M}}(\boldsymbol{\kappa}_\mathbf{r}) - \widetilde{\mathsf{J}}(\boldsymbol{\kappa}_\mathbf{r})\right]. \quad (14)$$

By applying the Fourier transform to (7) we obtain

$$\widetilde{\mathsf{J}}_\mathrm{s}^{(m)}(\boldsymbol{\kappa}) = \frac{1}{(2\pi)^3} \int_{\mathcal{R}^3} \underline{\widetilde{\mathsf{D}}}_\mathrm{JE}^{(m)}(\boldsymbol{\kappa}, \overline{\boldsymbol{\kappa}})\, \widetilde{\mathsf{E}}_\mathrm{t}(\overline{\boldsymbol{\kappa}})\, d\overline{\boldsymbol{\kappa}} + \frac{1}{(2\pi)^3} \int_{\mathcal{R}^3} \underline{\widetilde{\mathsf{D}}}_\mathrm{JH}^{(m)}(\boldsymbol{\kappa}, \overline{\boldsymbol{\kappa}})\, \widetilde{\mathsf{H}}_\mathrm{t}(\overline{\boldsymbol{\kappa}})\, d\overline{\boldsymbol{\kappa}} \quad (15)$$

where $\underline{\widetilde{\mathsf{D}}}_\mathrm{JE}^{(m)}(\boldsymbol{\kappa}, \overline{\boldsymbol{\kappa}})$ and $\underline{\widetilde{\mathsf{D}}}_\mathrm{JH}^{(m)}(\boldsymbol{\kappa}, \overline{\boldsymbol{\kappa}})$ take the role of the *bi-frequency system functions*, or *mapping functions*, in analogy with the bi-frequency system function of time-variant systems [33]. They give the induced current response of the EMO at wavenumber $\boldsymbol{\kappa}$ when a plane wave with wavenumber $\overline{\boldsymbol{\kappa}}$ is applied at the input. Similar expressions hold for $\widetilde{\mathsf{M}}_\mathrm{s}^{(m)}(\boldsymbol{\kappa})$, $\underline{\widetilde{\mathsf{D}}}_\mathrm{JE}^{(m)}(\boldsymbol{\kappa}, \overline{\boldsymbol{\kappa}})$, $\underline{\widetilde{\mathsf{D}}}_\mathrm{JH}^{(m)}(\boldsymbol{\kappa}, \overline{\boldsymbol{\kappa}})$, $\underline{\widetilde{\mathsf{D}}}_\mathrm{ME}^{(m)}(\boldsymbol{\kappa}, \overline{\boldsymbol{\kappa}})$, and $\underline{\widetilde{\mathsf{D}}}_\mathrm{MH}^{(m)}(\boldsymbol{\kappa}, \overline{\boldsymbol{\kappa}})$, which depend on EMO's characteristics and configuration and might represent the optimization objective in a reconfigurable EM system, as it will be shown in the sequel. Due to the presence of feedback, they impose the boundary conditions that are responsible for the presence of field discontinuity. This aspect will be discussed in Sec. VI.

D. EM Transfer Function

In analogy with the transfer function of linear filters, the Fourier representation gives the possibility to define the (space-variant) *EM transfer function* $\underline{\widetilde{\mathcal{H}}}(\boldsymbol{\kappa}, \overline{\boldsymbol{\kappa}})$ of the system that relates the impressed currents (input) and the resulting EM field (output) in the wavenumber domain. Typically, only the impressed electric currents and the electric field are considered then, without loss of generality, we focus on the EM transfer function component $\underline{\widetilde{\mathcal{H}}}_\mathrm{EJ}(\boldsymbol{\kappa}, \overline{\boldsymbol{\kappa}})$ that relates $\widetilde{\mathsf{J}}_\mathrm{imp}(\boldsymbol{\kappa}) = \sum_m \widetilde{\mathsf{J}}_\mathrm{imp}^{(m)}(\boldsymbol{\kappa})$ and the electric field $\widetilde{\mathsf{E}}(\boldsymbol{\kappa})$. In general, being the system space variant, $\widetilde{\mathsf{E}}(\boldsymbol{\kappa})$ can be expressed as

$$\widetilde{\mathsf{E}}(\boldsymbol{\kappa}) = \frac{1}{(2\pi)^3} \int_{\mathcal{R}^3} \underline{\widetilde{\mathcal{H}}}_\mathrm{EJ}(\boldsymbol{\kappa}, \overline{\boldsymbol{\kappa}})\, \widetilde{\mathsf{J}}_\mathrm{imp}(\overline{\boldsymbol{\kappa}})\, d\overline{\boldsymbol{\kappa}}. \quad (16)$$

The EM transfer function $\underline{\widetilde{\mathcal{H}}}_\mathrm{EJ}(\boldsymbol{\kappa}, \overline{\boldsymbol{\kappa}})$ indicates what is the response of the entire system at wavenumber $\boldsymbol{\kappa}$ when it is solicited by an impressed current with wavenumber $\overline{\boldsymbol{\kappa}}$. Specifically, the component $\widetilde{\mathcal{H}}_\mathrm{EJ}^{(xx)}(\boldsymbol{\kappa}, \overline{\boldsymbol{\kappa}})$ of $\underline{\widetilde{\mathcal{H}}}_\mathrm{EJ}(\boldsymbol{\kappa}, \overline{\boldsymbol{\kappa}})$ represents the response of the system at polarization $\hat{\mathbf{a}}_x$ when solicited by the *harmonic current* $\widetilde{\mathsf{J}}_\mathrm{imp}(\boldsymbol{\kappa}) = \hat{\mathbf{a}}_x (2\pi)^3 \delta(\boldsymbol{\kappa} - \overline{\boldsymbol{\kappa}})$ generating a plane wave with wavenumber $\overline{\boldsymbol{\kappa}}$. Similarly for the other polarization combinations. Note that the harmonic current is a dual of the infinitesimal source current, and it has only a mathematical meaning.

E. Information Theoretic Channel Matrix

The appeal of IT lies in its agnostic approach towards the physical interpretation of signals used as input and output in communication systems. However, to obtain physically consistent results, it is essential to establish a correct mapping with EM quantities, which is crucial for deriving fundamental bounds and for the design process. Let $\mathbf{x} \in \mathbb{C}^P$ and $\mathbf{y} \in \mathbb{C}^Q$ be the vectors representing the P inputs and Q outputs of the multiple-input multiple-output (MIMO) channel adopted in IT or signal processing frameworks. Typically, their relationship is modeled as follows:

$$\mathbf{y} = \mathbf{H}\,\mathbf{x} + \mathbf{n} \quad (17)$$

where $\mathbf{H} \in \mathbb{C}^{Q \times P}$ is the *IT channel matrix*, $\mathbf{n} \in \mathbb{C}^Q \sim \mathcal{N}_\mathrm{c}\left(\mathbf{0}_{1\times Q}, \sigma^2 \mathbf{I}_Q\right)$ is the additive white Gaussian noise (AWGN) with σ^2 being the thermal noise power. It is well-known from MIMO theory that one fundamental parameter affecting the capacity of the communication system, given a constraint on the transmitted power $\mathbb{E}\left\{\|\mathbf{x}\|^2\right\}$, is represented by the rank of the channel matrix $\mathbf{H}$. The MIMO model in (17) acquires a physical meaning if a proper isomorphism is considered between the IT signals, $\mathbf{x}$ and $\mathbf{y}$, and the voltages at the antenna ports $\mathbf{v}$ and $\mathbf{u}$, thus making the channel matrix $\mathbf{H}$ physically consistent. This can be achieved, as proposed in [34], by considering the insertion of a power-matching network at the transmitter and a noise-matching network at the receiver, as shown in Fig. 1. Denoting with $\mathbf{v}_\mathrm{T}$ and $\mathbf{v}_\mathrm{L}$ the voltage vectors, respectively, at the input and output of the matching networks, the following isomorphism $\mathbf{x} = \mathbf{v}_\mathrm{T}/\sqrt{2R}$ and $\mathbf{y} = \sigma\, \mathbf{C}_\mathrm{R}^{-1/2} \mathbf{v}_\mathrm{L}/\sqrt{2R}$, with R being the matching resistance, leads to

$$\mathbf{H} = \left(\Re\left\{\mathbf{Z}_\mathrm{R}\right\}\right)^{-\frac{1}{2}} \mathbf{Z}_\mathrm{C} \left(\Re\left\{\mathbf{Z}_\mathrm{T}\right\}\right)^{-\frac{1}{2}} \quad (18)$$

where the operator $\Re\{x\}$ denotes the real part of x, $\mathbf{Z}_\mathrm{C}$ is the transimpedance matrix modeling the mutual coupling between the receiving and transmitting antennas, and $\mathbf{C}_\mathrm{R}$ is the covariance matrix of the thermal noise component in $\mathbf{v}_\mathrm{L}$ which is a function of the impedance matrices $\mathbf{Z}_\mathrm{C}$ and $\mathbf{Z}_\mathrm{R}$, as well as of the characteristics of the extrinsic and intrinsic noise (caused by the background radiation and by the receiver power amplifiers, respectively), as shown in [34]. In particular, it is $\mathbf{u}|_{\mathbf{j}=0} = \mathbf{Z}_\mathrm{C}\,\mathbf{i}$, where $\mathbf{u}|_{\mathbf{j}=0}$ is the open circuit output voltage and $\mathbf{i}$ the input current. The previous isomorphism ensures that the noise components of $\mathbf{n}$ in (17) are independent, and $\mathbb{E}\left\{\|\mathbf{x}\|^2\right\}$ corresponds effectively to the transmitted power $P_\mathrm{T} = \mathbb{E}\left\{\|\mathbf{v}_\mathrm{T}\|^2\right\}/2R = \mathbb{E}\left\{\|\mathbf{x}\|^2\right\}$ that, assuming a lossless device, is equal to the radiated power P_rad. In the following sections (Secs. III, IV, V, and VI), we present an approach, based on linear algebra, to compute efficiently the EM transfer function and the IT channel matrix in (16) and (18) that allows to easily incorporate design, analysis, and optimization problems involving reconfigurable EMOs. The relationship between the EM transfer function and the IT channel matrix as well as an approach to compute the coupling matrices and the antennas DoF will be given in Secs. VII and VIII.

III. Linear Algebra Formulation

The following approach takes inspiration from the well-known method of moments or mode matching [35]. For convenience, we introduce the inner product between vector functions $\mathsf{A}(\mathbf{r})$ and $\mathsf{B}(\mathbf{r})$, defined on the generic surface $\mathcal{S}$, as

$$\langle \mathsf{A}(\mathbf{r}), \mathsf{B}(\mathbf{r}) \rangle = \int_\mathcal{S} \mathsf{A}(\mathbf{r}) \cdot \mathsf{B}^*(\mathbf{r})\, d\mathbf{r}. \quad (19)$$

Suppose $\left\{\boldsymbol{\Phi}_n^{(m)}(\mathbf{r})\right\}_{n=1}^{N^{(m)}}$ is a complete vector orthonormal basis set for $\mathcal{S}^{(m)}$. The orthogonality condition implies that $\left\langle \boldsymbol{\Phi}_n^{(m)}(\mathbf{r}), \boldsymbol{\Phi}_i^{(m)}(\mathbf{r}) \right\rangle = \delta_{n,i}$. It is worth noticing that $\boldsymbol{\Phi}_n^{(m)}(\mathbf{r})$ is a 3D vector which is tangent to the surface $\mathcal{S}^{(m)}$ for all $\mathbf{r} \in \mathcal{S}^{(m)}$ and zero otherwise. Moreover, all the basis sets refer to different surfaces so that $\left\langle \boldsymbol{\Phi}_u^{(m)}(\mathbf{r}), \boldsymbol{\Phi}_n^{(i)}(\mathbf{r}) \right\rangle = 0$, $\forall u, n$ and $i \neq m$. It follows that any vector function (field) $\mathsf{A}(\mathbf{r})$ lying on surface $\mathcal{S}^{(m)}$ can be represented as a linear combination of the basis functions (*modes*) composing the basis set[1]

$$\mathsf{A}(\mathbf{r}) = \sum_{n=1}^{N^{(m)}} a_n \, \boldsymbol{\Phi}_n^{(m)}(\mathbf{r}) \tag{20}$$

where the complex coefficients $\{a_n\}$ are given by $a_n = \left\langle \mathsf{A}(\mathbf{r}), \boldsymbol{\Phi}_n^{(m)}(\mathbf{r}) \right\rangle$, for $n = 1, 2, \ldots, N^{(m)}$. Accordingly, the components $\mathsf{J}^{(m)}(\mathbf{r})$ and $\mathsf{M}^{(m)}(\mathbf{r})$ can be represented in terms of the series expansions

$$\mathsf{J}^{(m)}(\mathbf{r}) = \sum_{n=1}^{N^{(m)}} b_{J_n}^{(m)} \, \boldsymbol{\Phi}_n^{(m)}(\mathbf{r}) + \sum_{n=1}^{N^{(m)}} a_{J_n}^{(m)} \, \boldsymbol{\Phi}_n^{(m)}(\mathbf{r}) \tag{21}$$

$$\mathsf{M}^{(m)}(\mathbf{r}) = \sum_{n=1}^{N^{(m)}} b_{M_n}^{(m)} \, \boldsymbol{\Phi}_n^{(m)}(\mathbf{r}) + \sum_{n=1}^{N^{(m)}} a_{M_n}^{(m)} \, \boldsymbol{\Phi}_n^{(m)}(\mathbf{r}) \tag{22}$$

where $a_{J_n}^{(m)} = \left\langle \mathsf{J}_{\text{imp}}^{(m)}(\mathbf{r}), \boldsymbol{\Phi}_n^{(m)}(\mathbf{r}) \right\rangle$, $b_{J_n}^{(m)} = \left\langle \mathsf{J}_{\text{s}}^{(m)}(\mathbf{r}), \boldsymbol{\Phi}_n^{(m)}(\mathbf{r}) \right\rangle$, $a_{M_n}^{(m)} = \left\langle \mathsf{M}_{\text{imp}}^{(m)}(\mathbf{r}), \boldsymbol{\Phi}_n^{(m)}(\mathbf{r}) \right\rangle$, and $b_{M_n}^{(m)} = \left\langle \mathsf{M}_{\text{s}}^{(m)}(\mathbf{r}), \boldsymbol{\Phi}_n^{(m)}(\mathbf{r}) \right\rangle$. Denote with $\mathbf{a}_J^{(m)} = \left[\left\{a_{J_n}^{(m)}\right\}\right]$, $\mathbf{b}_J^{(m)} = \left[\left\{b_{J_n}^{(m)}\right\}\right]$, $\mathbf{a}_M^{(m)} = \left[\left\{a_{M_n}^{(m)}\right\}\right]$, $\mathbf{b}_M^{(m)} = \left[\left\{b_{M_n}^{(m)}\right\}\right]$ the column vectors collecting the coefficients in (21) and (22), respectively. We define also the vectors $\mathbf{a}^{(m)} = \left[\, \mathbf{a}_J^{(m)T} \;\; \mathbf{a}_M^{(m)T} \right]^T$ and $\mathbf{b}^{(m)} = \left[\mathbf{b}_J^{(m)T} \;\; \mathbf{b}_M^{(m)T}\right]^T$.

By applying the inner product to both sides of (1) with the nth basis function $\boldsymbol{\Phi}_n^{(m)}(\mathbf{r})$ of the generic mth EMO, and by exploiting (21)-(22) as well as the orthogonality condition, we obtain

$$\begin{aligned}
e_n^{(m)} &= \left\langle \mathsf{E}(\mathbf{r}), \boldsymbol{\Phi}_n^{(m)}(\mathbf{r}) \right\rangle = \left\langle \mathsf{E}_{\text{t}}^{(m)}(\mathbf{r}), \boldsymbol{\Phi}_n^{(m)}(\mathbf{r}) \right\rangle \\
&= \left\langle \underline{\mathsf{G}}_{\text{EJ}} \cdot \mathsf{J}(\mathbf{r}), \boldsymbol{\Phi}_n^{(m)}(\mathbf{r}) \right\rangle + \left\langle \underline{\mathsf{G}}_{\text{EM}} \cdot \mathsf{M}(\mathbf{r}), \boldsymbol{\Phi}_n^{(m)}(\mathbf{r}) \right\rangle \\
&= \sum_{i=1}^{M} \left\langle \underline{\mathsf{G}}_{\text{EJ}} \cdot \mathsf{J}^{(i)}(\mathbf{r}), \boldsymbol{\Phi}_n^{(m)}(\mathbf{r}) \right\rangle \\
&\quad + \sum_{i=1}^{M} \left\langle \underline{\mathsf{G}}_{\text{EM}} \cdot \mathsf{M}^{(i)}(\mathbf{r}), \boldsymbol{\Phi}_n^{(m)}(\mathbf{r}) \right\rangle \\
&= \sum_{i=1}^{M} \sum_{u=1}^{N^{(i)}} \left(a_{J_u}^{(i)} + b_{J_u}^{(i)}\right) \left\langle \underline{\mathsf{G}}_{\text{EJ}} \cdot \boldsymbol{\Phi}_u^{(i)}(\mathbf{r}), \boldsymbol{\Phi}_n^{(m)}(\mathbf{r}) \right\rangle \\
&\quad + \sum_{i=1}^{M} \sum_{u=1}^{N^{(i)}} \left(a_{M_u}^{(i)} + b_{M_u}^{(i)}\right) \left\langle \underline{\mathsf{G}}_{\text{EM}} \cdot \boldsymbol{\Phi}_u^{(i)}(\mathbf{r}), \boldsymbol{\Phi}_n^{(m)}(\mathbf{r}) \right\rangle .
\end{aligned} \tag{23}$$

[1]In general, $N^{(m)}$ could be infinity for the basis set to be complete. In such a case, $N^{(m)}$ can be set to a finite value sufficiently large according to the desired level of accuracy.

Similarly for the magnetic field component

$$\begin{aligned}
h_n^{(m)} &= \left\langle \mathsf{H}(\mathbf{r}), \boldsymbol{\Phi}_n^{(m)}(\mathbf{r}) \right\rangle = \left\langle \mathsf{H}_{\text{t}}^{(m)}(\mathbf{r}), \boldsymbol{\Phi}_n^{(m)}(\mathbf{r}) \right\rangle \\
&= \sum_{i=1}^{M} \sum_{u=1}^{N^{(i)}} \left(a_{J_u}^{(i)} + b_{J_u}^{(i)}\right) \left\langle \underline{\mathsf{G}}_{\text{HJ}} \cdot \boldsymbol{\Phi}_u^{(i)}(\mathbf{r}), \boldsymbol{\Phi}_n^{(m)}(\mathbf{r}) \right\rangle \\
&\quad + \sum_{i=1}^{M} \sum_{u=1}^{N^{(i)}} \left(a_{M_u}^{(i)} + b_{M_u}^{(i)}\right) \left\langle \underline{\mathsf{G}}_{\text{HM}} \cdot \boldsymbol{\Phi}_u^{(i)}(\mathbf{r}), \boldsymbol{\Phi}_n^{(m)}(\mathbf{r}) \right\rangle .
\end{aligned} \tag{24}$$

As a consequence, the EM field $\left(\mathsf{E}_{\text{t}}^{(m)}(\mathbf{r}), \mathsf{H}_{\text{t}}^{(m)}(\mathbf{r})\right)$ tangent to the surface $\mathcal{S}^{(m)}$ can be expressed according to the series expansions

$$\mathsf{E}_{\text{t}}^{(m)}(\mathbf{r}) = \sum_{n=1}^{N^{(m)}} e_n^{(m)} \, \boldsymbol{\Phi}_n^{(m)}(\mathbf{r}) \qquad \mathsf{H}_{\text{t}}^{(m)}(\mathbf{r}) = \sum_{n=1}^{N^{(m)}} h_n^{(m)} \, \boldsymbol{\Phi}_n^{(m)}(\mathbf{r}). \tag{25}$$

Note that the above series expansion is valid only for the EM field tangent to the surface. Define the vector $\mathbf{f}^{(m)} = \left[\mathbf{e}^{(m)T} \, \mathbf{h}^{(m)T}\right]^T$ of dimension $2N^{(m)}$, with $\mathbf{e}^{(m)} = \left[\left\{e_n^{(m)}\right\}\right]$ and $\mathbf{h}^{(m)} = \left[\left\{h_n^{(m)}\right\}\right]$ being the column vectors collecting the coefficients in (25). By considering (23) and (24), $\mathbf{f}^{(m)}$ can be written in matrix form as

$$\mathbf{f}^{(m)} = \sum_{i=1}^{M} \mathbf{G}^{(m,i)} \left[\mathbf{b}^{(i)} + \mathbf{a}^{(i)}\right] \tag{26}$$

where

$$\mathbf{G}^{(m,i)} = \begin{bmatrix} \mathbf{G}_{\text{EJ}}^{(m,i)} & \mathbf{G}_{\text{EM}}^{(m,i)} \\ \mathbf{G}_{\text{HJ}}^{(m,i)} & \mathbf{G}_{\text{HM}}^{(m,i)} \end{bmatrix} \tag{27}$$

is the coupling matrix of dimension $2N^{(m)} \times 2N^{(i)}$, whose elements are given by

$$\left[\mathbf{G}_{\text{EJ}}^{(m,i)}\right]_{u,n} = \left\langle \underline{\mathsf{G}}_{\text{EJ}} \boldsymbol{\Phi}_u^{(i)}(\mathbf{r}), \boldsymbol{\Phi}_n^{(m)}(\mathbf{r}) \right\rangle \tag{28}$$

$$= \frac{1}{\jmath\omega\epsilon} \int_{\mathcal{S}^{(m)}} \left(\boldsymbol{\Phi}_n^{(m)}(\mathbf{r})\right)^* \tag{29}$$

$$\cdot \nabla_{\mathbf{x}} \nabla_{\mathbf{x}} \int_{\mathcal{S}^{(i)}} G_0(\mathbf{r}-\mathbf{s}) \, \boldsymbol{\Phi}_u^{(i)}(\mathbf{s}) \, d\mathbf{s} \, d\mathbf{r} \tag{30}$$

$$\left[\mathbf{G}_{\text{EM}}^{(m,i)}\right]_{u,n} = \left\langle \underline{\mathsf{G}}_{\text{EM}} \boldsymbol{\Phi}_u^{(i)}(\mathbf{r}), \boldsymbol{\Phi}_n^{(m)}(\mathbf{r}) \right\rangle \tag{31}$$

$$= -\int_{\mathcal{S}^{(m)}} \left(\boldsymbol{\Phi}_n^{(m)}(\mathbf{r})\right)^* \cdot \nabla_{\mathbf{x}} \int_{\mathcal{S}^{(i)}} G_0(\mathbf{r}-\mathbf{s}) \, \boldsymbol{\Phi}_u^{(i)}(\mathbf{s}) \, d\mathbf{s} \, d\mathbf{r} \tag{32}$$

$$\left[\mathbf{G}_{\text{HJ}}^{(m,i)}\right]_{u,n} = \left\langle \underline{\mathsf{G}}_{\text{HJ}} \boldsymbol{\Phi}_u^{(i)}(\mathbf{r}), \boldsymbol{\Phi}_n^{(m)}(\mathbf{r}) \right\rangle = -\left[\mathbf{G}_{\text{EM}}^{(m,i)}\right]_{u,n} \tag{33}$$

$$\left[\mathbf{G}_{\text{HM}}^{(m,i)}\right]_{u,n} = \left\langle \underline{\mathsf{G}}_{\text{HM}} \boldsymbol{\Phi}_u^{(i)}(\mathbf{r}), \boldsymbol{\Phi}_n^{(m)}(\mathbf{r}) \right\rangle = \frac{\epsilon}{\mu} \left[\mathbf{G}_{\text{EJ}}^{(m,i)}\right]_{u,n} \tag{34}$$

for $n = 1, 2, \ldots, N^{(m)}$, $u = 1, 2, \ldots, N^{(i)}$. It is worth noticing that the coupling matrices above depend only on the reciprocal geometry between EMOs i and m, i.e., their

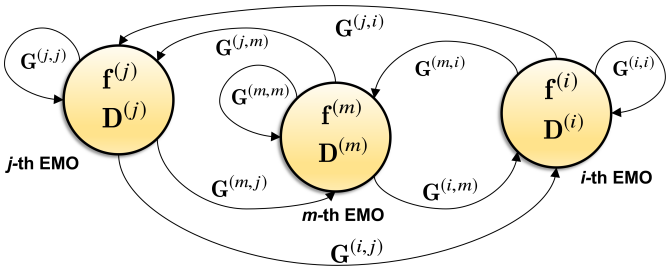

Fig. 2. EM scenario as a fully connected graph.

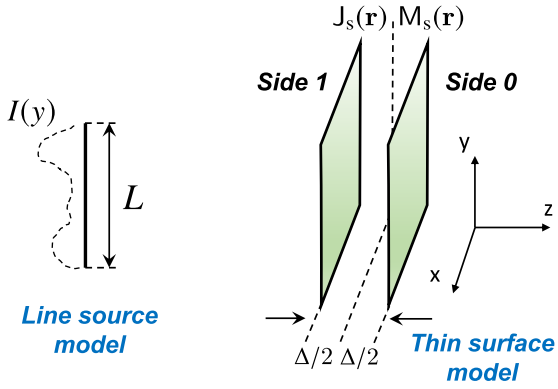

Fig. 3. Line source (left) and thin surface models (right).

relative position and orientation. When $i = m$ (self-coupling), they depend neither on the position nor on the orientation. When the coupling between EMOs m and i is negligible, $\mathbf{G}_{\mathrm{EJ}}^{(m,i)}, \mathbf{G}_{\mathrm{EM}}^{(m,i)}, \mathbf{G}_{\mathrm{HM}}^{(m,i)}, \mathbf{G}_{\mathrm{HJ}}^{(m,i)} \approx \mathbf{0}_{2N^{(m)} \times 2N^{(i)}}$. Following a similar approach, also the constitutive equation (7) can be put in matrix form

$$\mathbf{b}^{(m)} = \mathbf{D}^{(m)}\, \mathbf{f}^{(m)} \qquad \text{where} \quad \mathbf{D}^{(m)} = \begin{bmatrix} \mathbf{D}_{\mathrm{JE}}^{(m)} & \mathbf{D}_{\mathrm{JH}}^{(m)} \\ \mathbf{D}_{\mathrm{ME}}^{(m)} & \mathbf{D}_{\mathrm{MH}}^{(m)} \end{bmatrix} \tag{35}$$

and

$$\left[\mathbf{D}_{\mathrm{JE}}^{(m)}\right]_{u,n} = \left\langle \underline{\mathsf{D}}_{\mathrm{JE}}^{(m)} \cdot \boldsymbol{\Phi}_u^{(m)}(\mathbf{r}), \boldsymbol{\Phi}_n^{(m)}(\mathbf{r}) \right\rangle \tag{36}$$

$$\left[\mathbf{D}_{\mathrm{JH}}^{(m)}\right]_{u,n} = \left\langle \underline{\mathsf{D}}_{\mathrm{JH}}^{(m)} \cdot \boldsymbol{\Phi}_u^{(m)}(\mathbf{r}), \boldsymbol{\Phi}_n^{(m)}(\mathbf{r}) \right\rangle \tag{37}$$

$$\left[\mathbf{D}_{\mathrm{ME}}^{(m)}\right]_{u,n} = \left\langle \underline{\mathsf{D}}_{\mathrm{ME}}^{(m)} \cdot \boldsymbol{\Phi}_u^{(m)}(\mathbf{r}), \boldsymbol{\Phi}_n^{(m)}(\mathbf{r}) \right\rangle \tag{38}$$

$$\left[\mathbf{D}_{\mathrm{MH}}^{(m)}\right]_{u,n} = \left\langle \underline{\mathsf{D}}_{\mathrm{MH}}^{(m)} \cdot \boldsymbol{\Phi}_u^{(m)}(\mathbf{r}), \boldsymbol{\Phi}_n^{(m)}(\mathbf{r}) \right\rangle \tag{39}$$

with $u, n = 1, 2, \ldots N^{(m)}$. Matrix $\mathbf{D}^{(m)}$, of dimension $2N^{(m)} \times 2N^{(m)}$, describes completely the linear transformation operated by the mth EMO, polarization effects included, under the limit of the series expansion approximation.

For instance, if we are interested in finding the EM field tangent to the surface $\mathcal{S}^{(m)}$ of the mth EMO, by combining (26) and (35), it is

$$\mathbf{f}^{(m)} = \left(\mathbf{I} - \mathbf{G}^{(m,m)}\mathbf{D}^{(m)}\right)^{-1} \cdot \left(\sum_{i=1, i\neq m}^{M} \mathbf{G}^{(m,i)}\mathbf{D}^{(i)}\mathbf{f}^{(i)} + \sum_{i=1}^{M} \mathbf{G}^{(m,i)}\mathbf{a}^{(i)} \right). \tag{40}$$

Once such coefficients have been derived, the corresponding field can be obtained using (25).

The matrix relationships above can be graphically represented as a connected graph sketched in Fig. 2. Graph theory tools, such as the Mason's gain formula [36], can be exploited to solve (40) or any other set of equations depending on the structure of the system. Significant simplifications can be operated if the coupling between some EMOs is weak and/or the induced currents at any EMO are negligible. Matrix representation is useful in optimization problems where the best configuration of one or more EMOs, i.e., their matrix $\mathbf{D}$, must be found to achieve a given result on the EM field. Some examples will be provided in Sec. VIII.

IV. Basis Sets and Sources

A crucial aspect of the linear algebra formulation illustrated in the previous section is the choice of the basis functions and their number that affect the trade-off between accuracy and computational complexity [29], [31]. We choose the harmonic basis functions, which allow for an efficient representation and the possibility to exploit the properties of the Fourier analysis. Without loss of generality, we consider EMOs oriented according to the plane $z = 0$ and centered at the origin (canonical position and orientation). How to deal with differently oriented and positioned EMOs will be explained at the end of the section. In the following, we illustrate possible basis sets for some geometries of interest.

A. Infinitesimal Vertically Polarized Current Source

Considering a canonical vertical polarization, the only possible base function is $\boldsymbol{\Phi}_1(\mathbf{r}) = \hat{\mathbf{y}}\, \delta(x)\, \delta(y)\, \delta(z)$ so that $\widetilde{\boldsymbol{\Phi}}_1(\boldsymbol{\kappa}) = \mathcal{F}[\boldsymbol{\Phi}_1(\mathbf{r})] = \hat{\mathbf{y}}$. The infinitesimal source is typically used to model the small dipole of infinitesimal length ΔL and current I_0 whose current density can be written as $\mathsf{J}(\mathbf{r}) = \hat{\mathbf{y}} I_0\, \Delta L\, \boldsymbol{\Phi}_1(\mathbf{r})$ and $\widetilde{\mathsf{J}}(\boldsymbol{\kappa}) = I_0\, \Delta L\, \widetilde{\boldsymbol{\Phi}}_1(\boldsymbol{\kappa})$ (Hertzian dipole) [29, Ch. 4].

B. Line Source of Length L

An example of a line source, shown in Fig. 3, is given by the conducting wire of length L. In this case we have $\mathsf{J}(\mathbf{r}) = \hat{\mathbf{y}}\, I(y)\, \delta(x)\, \delta(z)$, with current distribution $I(y)$ different from zero in $|y| < L/2$. The basis functions are $\boldsymbol{\Phi}_n(\mathbf{r}) = \hat{\mathbf{y}}\, \phi_n(\mathbf{r})$, where $\phi_n(\mathbf{r})$ are scalar basis functions for $n = 1, 2, \ldots, N_y$ (N_y odd number). For convenience and with some abuse of notation, consider also the following alternative indexing $\boldsymbol{\Phi}_{n_y}(\mathbf{r})$, where n_y is related to n according to the mapping $n_y = n - (N_y - 1)/2 - 1$, for $n_y = -(N_y - 1)/2, \ldots, -1, 0, 1, \ldots, (N_y - 1)/2$. A complete basis set for a vertical line of length L, with $y \in [L/2, L/2]$, is given by $\phi_{n_y}(\mathbf{r}) = I_{n_y}(y; L)\, \delta(x)\, \delta(z)$, having defined $I_{n_y}(y; L) = \frac{1}{\sqrt{L}} \mathrm{Rect}\left(\frac{y}{L}\right) \exp\left(\jmath \frac{2\pi n_y y}{L}\right)$, where the coefficient ensures that the basis functions have unitary energy. In the frequency domain, we have $\widetilde{\boldsymbol{\Phi}}_{n_y}(\boldsymbol{\kappa}) = \hat{\mathbf{y}}\, \tilde{\phi}_{n_y}(\boldsymbol{\kappa}; L)$, with $\tilde{\phi}_{n_y}(\boldsymbol{\kappa}; L) = \tilde{\phi}_{n_y}(k_y; L) = S_{n_y}(k_y; L)$, where

$$S_n(k; L) = \sqrt{L}\, \mathrm{Sinc}\left(\frac{k\, L}{2\pi} - n\right). \tag{41}$$

C. Thin Surface of Size $L_x \times L_y$

A thin RIS that is electrically large and made of sub-wavelength reconfigurable scattering elements, is

homogenizable and can be modeled as a continuous surface sheet characterized by suitable surface functions (in general dyadic tensors) such as impedances or admittances (impedance sheet) [22]. Therefore, it is of interest to define a basis set to express any surface function. By applying the basis functions in (41) to each dimension of the surface, any scalar surface function can be represented as a linear combination of the following scalar basis functions

$$\phi_{n_x,n_y}(\mathbf{r}) = I_{n_x}(x;L_x)\, I_{n_y}(y;L_y)\, \delta(z) \tag{42}$$

$$\tilde{\phi}_{n_x,n_y}(\boldsymbol{\kappa}) = \mathcal{F}\left[\phi_{n_x,n_y}(\mathbf{r})\right] = S_{n_x}(k_x;L_x)\, S_{n_y}(k_y;L_y) \tag{43}$$

respectively, in the spatial and wavenumber domains, with $n_x = -(N_x-1)/2,\ldots,-1,0,1,\ldots,(N_x-1)/2$, $n_y = -(N_y-1)/2,\ldots,-1,0,1,\ldots,(N_y-1)/2$.

The currents induced by the incident EM field introduce a discontinuity in the EM fields on the two sides of the surface. Therefore, we model it with two separate faces (sides) at infinitesimal distance Δ at $z = -\Delta/2$ and $z = \Delta/2$, where $\Delta \ll \lambda$ is the thickness of the surface, as shown in Fig. 3. To condense the notation, with introduce the alternative indexing $n = n_x+(N_x-1)/2+1+N_x(n_y+(N_y-1)/2)+n_pN_xN_y+n_s2N_xN_y$, where $n_p = 0$ if horizontally polarized and $n_p = 1$ if vertically polarized, $n_s = 0$ if right-side face, and $n_s = 1$ if left-side face. In this manner, the complete basis set sufficient to represent any EM field on the two sides of the surface is

$$\begin{aligned}\boldsymbol{\Phi}_n(\mathbf{r}) &= \boldsymbol{\Phi}_{n_x,n_y,n_p,n_s}(\mathbf{r})\\ &= \hat{\mathbf{a}}_{n_p}\,\phi_{n_x,n_y}(\mathbf{r}+(0.5-n_s)\,\Delta\,\hat{\mathbf{z}})\end{aligned} \tag{44}$$

$$\widetilde{\boldsymbol{\Phi}}_{n_x,n_y,n_p,n_s}(\boldsymbol{\kappa}) = \hat{\mathbf{a}}_{n_p}\,\tilde{\phi}_{n_x,n_y}(\boldsymbol{\kappa})\, e^{J\kappa_z(0.5-n_s)\Delta} \tag{45}$$

where $\hat{\mathbf{a}}_{n_p} = \hat{\mathbf{x}}$, when $n_p = 0$, and $\hat{\mathbf{a}}_{n_p} = \hat{\mathbf{y}}$, when $n_p = 1$. Therefore, the total number of basis functions is $N = 4N_xN_y$. Currents are supposed to lay at $z = 0$, i.e., in the middle of the two sides, to avoid singularities, and hence $2N_xN_y$ basis functions are sufficient to represent them.

D. Basis Functions for Plane Waves and Elementary Harmonic Currents

To create a "bridge" between the linear algebra characterization in Sec. III and the EM transfer function in (16), it is convenient to define a virtual EMO consisting of a generic plane wave with wavenumber $\overline{\boldsymbol{\kappa}} = (\overline{\kappa}_x, \overline{\kappa}_y, \overline{\kappa}_z)$ and polarization $\hat{\mathbf{a}}(\overline{\boldsymbol{\kappa}})$. As it will be clearer later, thanks to this virtual EMO, it is possible to determine how the system is coupled with the EM field at the generic wavenumber $\overline{\boldsymbol{\kappa}}$. In other words, it can be used to "observe" the EM field without any influence on it. Any plane wave can be fully represented as a linear combination of two basis functions $\boldsymbol{\Phi}_n(\mathbf{r};\overline{\boldsymbol{\kappa}}) = \hat{\mathbf{a}}_n(\overline{\boldsymbol{\kappa}})\, e^{J\overline{\boldsymbol{\kappa}}\cdot\mathbf{r}}$, where the vectors $\hat{\mathbf{a}}_1(\overline{\boldsymbol{\kappa}})$ and $\hat{\mathbf{a}}_2(\overline{\boldsymbol{\kappa}})$ are, respectively, transversal and longitudinal with respect to the direction of propagation $\overline{\boldsymbol{\kappa}}$ since it should be $\overline{\boldsymbol{\kappa}}\cdot\hat{\mathbf{a}}(\overline{\boldsymbol{\kappa}}) = 0$ [32]. Taking the Fourier transform, it is

$$\widetilde{\boldsymbol{\Phi}}_n(\boldsymbol{\kappa};\overline{\boldsymbol{\kappa}}) = (2\pi)^3\hat{\mathbf{a}}_n(\overline{\boldsymbol{\kappa}})\,\delta(\boldsymbol{\kappa}-\overline{\boldsymbol{\kappa}}). \tag{46}$$

It is also of utility the definition of the plane wave observed on the $x-y$ plane at $z = z_o$, that is, $\boldsymbol{\Phi}_n(\mathbf{r};\overline{\boldsymbol{\kappa}},z_o) = \hat{\mathbf{a}}_n(\overline{\boldsymbol{\kappa}})\,\delta(z-z_o)\,e^{J\overline{\boldsymbol{\kappa}}\cdot\mathbf{r}}$, with $\hat{\mathbf{a}}_1(\overline{\boldsymbol{\kappa}}) = \hat{\mathbf{x}}$ and $\hat{\mathbf{a}}_2(\overline{\boldsymbol{\kappa}}) = \hat{\mathbf{y}}$, whose 2D Fourier transform, for $n = 1, 2$, is

$$\widetilde{\boldsymbol{\Phi}}_n(\kappa_x,\kappa_y;\overline{\boldsymbol{\kappa}},z_o) = (2\pi)^2\hat{\mathbf{a}}_n(\overline{\boldsymbol{\kappa}})\,\delta(\kappa_x-\overline{\kappa}_x)\,\delta(\kappa_y-\overline{\kappa}_y)\,e^{-J\overline{\kappa}_z z_o}. \tag{47}$$

Analogously, we can define the elementary harmonic electric current with polarization $\hat{\mathbf{a}}$ and wavenumber $\overline{\boldsymbol{\kappa}}$ flowing on the $x-y$ plane at $z = z_s$ having the 2D Fourier transform

$$\widetilde{\boldsymbol{\Phi}}(\kappa_x,\kappa_y;\overline{\boldsymbol{\kappa}},z_s) = (2\pi)^2\hat{\mathbf{a}}\,\delta(\kappa_x-\overline{\kappa}_x)\,\delta(\kappa_y-\overline{\kappa}_y)\,e^{-J\overline{\kappa}_z z_s}. \tag{48}$$

E. EMOs in Non-Canonical Position and Orientation

The basis functions in the wavenumber domain for EMOs with generic position $\mathbf{p}$ and orientation can be easily obtained by exploiting the Fourier transform property $\widetilde{\boldsymbol{\Phi}}(\boldsymbol{\kappa}) = \underline{\mathsf{R}}\cdot\breve{\boldsymbol{\Phi}}(\mathbf{R}\cdot\boldsymbol{\kappa})\,e^{-J\mathbf{p}\cdot\boldsymbol{\kappa}}$, where $\breve{\boldsymbol{\Phi}}(\boldsymbol{\kappa})$ is the basis function in the wavenumber domain of the EMO in the canonical position and orientation, $\mathbf{R}$ is the rotation matrix transformation [37], and $\underline{\mathsf{R}}$ is the corresponding polarization rotation dyadic.

V. Modes Coupling

The last ingredient necessary to implement the method based on linear algebra is the derivation of the coupling coefficients between modes composing the matrices $\mathbf{G}^{(m,i)}$. Since the coupling between basis functions belonging to the ith and m EMOs depends only on their relative position and orientation, it is convenient to consider $\widetilde{\boldsymbol{\Phi}}_u^{(i)}(\boldsymbol{\kappa}) = \breve{\boldsymbol{\Phi}}_u^{(i)}(\boldsymbol{\kappa})$ located at the origin (canonical position and orientation), and $\widetilde{\boldsymbol{\Phi}}_n^{(m)}(\boldsymbol{\kappa})$ at the relative position and orientation $\mathbf{p} = \mathbf{p}^{(m,i)} = \mathbf{p}^{(m)} - \mathbf{p}^{(i)}$ and $\mathbf{R}^{(m,i)}$, respectively, such that the two EMOs do not intersect along the z axis. By applying the Parseval's theorem to (28)-(34), it is

$$\begin{aligned}\left[\mathbf{G}_{\mathrm{EJ}}^{(m,i)}\right]_{u,n} &= \frac{J}{\omega\epsilon(2\pi)^3}\int_{\mathcal{R}^3}\widetilde{G}_0(\boldsymbol{\kappa})\left(\widetilde{\boldsymbol{\Phi}}_n^{(m)}(\boldsymbol{\kappa})\right)^*\cdot\left(\boldsymbol{\kappa}\times\boldsymbol{\kappa}\times\widetilde{\boldsymbol{\Phi}}_u^{(i)}(\boldsymbol{\kappa})\right)d\boldsymbol{\kappa}\\ &= \frac{J}{\omega\epsilon(2\pi)^3}\int_{\mathcal{R}^3}\widetilde{G}_0(\boldsymbol{\kappa})\,e^{J\mathbf{p}^{(m,i)}\cdot\boldsymbol{\kappa}}\\ &\quad\cdot\left(\underline{\mathsf{R}}^{(m,i)}\cdot\breve{\boldsymbol{\Phi}}_n^{(m)}\left(\mathbf{R}^{(m,i)}\cdot\boldsymbol{\kappa}\right)\right)^*\cdot\left(\boldsymbol{\kappa}\times\boldsymbol{\kappa}\times\breve{\boldsymbol{\Phi}}_u^{(i)}(\boldsymbol{\kappa})\right)d\boldsymbol{\kappa}\end{aligned} \tag{49}$$

$$\begin{aligned}\left[\mathbf{G}_{\mathrm{EM}}^{(m,i)}\right]_{u,n} &= -\frac{J}{(2\pi)^3}\int_{\mathcal{R}^3}\widetilde{G}_0(\boldsymbol{\kappa})\left(\widetilde{\boldsymbol{\Phi}}_n^{(m)}(\boldsymbol{\kappa})\right)^*\cdot\left(\boldsymbol{\kappa}\times\widetilde{\boldsymbol{\Phi}}_u^{(i)}(\boldsymbol{\kappa})\right)d\boldsymbol{\kappa}\\ &= -\frac{J}{(2\pi)^3}\int_{\mathcal{R}^3}\widetilde{G}_0(\boldsymbol{\kappa})\,e^{J\mathbf{p}^{(m,i)}\cdot\boldsymbol{\kappa}}\\ &\quad\cdot\left(\underline{\mathsf{R}}^{(m,i)}\cdot\breve{\boldsymbol{\Phi}}_n^{(m)}\left(\mathbf{R}^{(m,i)}\cdot\boldsymbol{\kappa}\right)\right)^*\cdot\left(\boldsymbol{\kappa}\times\breve{\boldsymbol{\Phi}}_u^{(i)}(\boldsymbol{\kappa})\right)d\boldsymbol{\kappa}.\end{aligned} \tag{50}$$

Using the equality (83) in the Appendix, alternative expressions for (49) and (50) can be obtained, respectively,

$$\begin{aligned}\left[\mathbf{G}_{\mathrm{EJ}}^{(m,i)}\right]_{u,n} &= \frac{\pi}{\omega\epsilon(2\pi)^3}\int_{\mathcal{R}^2}\frac{e^{J\mathbf{p}^{(m,i)}\cdot\boldsymbol{\kappa}^{\pm}}}{k_z(\kappa_x,\kappa_y)}\\ &\quad\cdot\left(\underline{\mathsf{R}}^{(m,i)}\cdot\breve{\boldsymbol{\Phi}}_n^{(m)}\left(\mathbf{R}^{(m,i)}\cdot\boldsymbol{\kappa}^{\pm}\right)\right)^*\\ &\quad\cdot\left(\boldsymbol{\kappa}^{\pm}\times\boldsymbol{\kappa}^{\pm}\times\breve{\boldsymbol{\Phi}}_u^{(i)}(\boldsymbol{\kappa}^{\pm})\right)d\kappa_x d\kappa_y\end{aligned} \tag{51}$$

$$\begin{aligned}\left[\mathbf{G}_{\mathrm{EM}}^{(m,i)}\right]_{u,n} &= -\frac{\pi}{(2\pi)^3}\int_{\mathcal{R}^2}\frac{e^{J\mathbf{p}^{(m,i)}\cdot\boldsymbol{\kappa}^{\pm}}}{k_z(\kappa_x,\kappa_y)}\\ &\quad\cdot\left(\underline{\mathsf{R}}^{(m,i)}\cdot\breve{\boldsymbol{\Phi}}_n^{(m)}\left(\mathbf{R}^{(m,i)}\cdot\boldsymbol{\kappa}^{\pm}\right)\right)^*\\ &\quad\cdot\left(\boldsymbol{\kappa}^{\pm}\times\breve{\boldsymbol{\Phi}}_u^{(i)}(\boldsymbol{\kappa}^{\pm})\right)d\kappa_x d\kappa_y\end{aligned} \tag{52}$$

where $k_z = k_z(\kappa_x, \kappa_y)$ and $\boldsymbol{\kappa}^{\pm}$ are defined in (84) and (85), respectively, with $r_z = p_z$ and $z_{\max} = z_{\min} = 0$. These alternate expressions are useful because they reduce the evaluation of the coupling coefficient to a 2D Fourier-type integral which can be numerically solved using efficient FFT tools. In the following, we derive further simplifications and closed-form expressions of the coupling coefficients for particular cases of interest.

A. Coupling Between Any EMOs in Far Field

When two EMOs are located in their respective far-field region, i.e., $L^2/|\mathbf{p}| \ll \lambda$, where L is the dimension of the largest EMO and $\mathbf{p} = \mathbf{p}^{(m,i)}$, the approximation (86) in the Appendix can be applied to (51) and (52) thus obtaining

$$\left[\mathbf{G}_{\mathrm{EJ}}^{(m,i)}\right]_{u,n} \simeq \jmath\, k_0\, \eta \frac{e^{\jmath\, k_0\, |\mathbf{p}|}}{4\pi\, |\mathbf{p}|} \left(\underline{\mathsf{R}}^{(m,i)} \cdot \breve{\boldsymbol{\Phi}}_n^{(m)}\left(\mathbf{R}^{(m,i)}\, \boldsymbol{\kappa}_{\mathbf{p}}\right)\right)^* \cdot \left(\hat{\mathbf{p}}^{\pm} \times \hat{\mathbf{p}}^{\pm} \times \breve{\boldsymbol{\Phi}}_u^{(i)}(\boldsymbol{\kappa}_{\mathbf{p}})\right) \tag{53}$$

$$\left[\mathbf{G}_{\mathrm{EM}}^{(m,i)}\right]_{u,n} \simeq -\jmath\, k_0 \frac{e^{\jmath\, k_0\, |\mathbf{p}|}}{4\pi\, |\mathbf{p}|} \left(\underline{\mathsf{R}}^{(m,i)} \cdot \breve{\boldsymbol{\Phi}}_n^{(m)}\left(\mathbf{R}^{(m,i)}\, \boldsymbol{\kappa}_{\mathbf{p}}\right)\right)^* \cdot \left(\hat{\mathbf{p}}^{\pm} \times \breve{\boldsymbol{\Phi}}_u^{(i)}(\boldsymbol{\kappa}_{\mathbf{p}})\right) \tag{54}$$

being $\boldsymbol{\kappa}_{\mathbf{p}} = k_0\, \hat{\mathbf{p}}^{\pm}$, where $\hat{\mathbf{p}}^{\pm} = (p_x, p_y, |p_z|)/|\mathbf{p}|$. Since $|\hat{\mathbf{p}}^{\pm}| = 1$, it is evident that only plane waves with $(\kappa_x, \kappa_y) \in \mathcal{P}$ contribute to the propagation in the far field of the EM wave.

B. Coupling With Plane Waves

When the mth EMO is a plane wave with wavenumber $\overline{\boldsymbol{\kappa}}$ and polarization $\hat{\mathbf{a}}_n(\overline{\boldsymbol{\kappa}})$, the coupling coefficients between the plane wave and the ith EMO can be obtained in closed form by substituting (46) in (49) and (50). Of more interest is the coupling with the wave plane in (47) at the observation plane $z = z_{\mathrm{o}}$ that can be easily obtained in closed form

$$\left[\mathbf{G}_{\mathrm{EJ}}^{(m,i)}\right]_{u,n} = \left[\mathbf{G}_{\mathrm{EJ}}^{(m,i)}\right]_{u,n}(\overline{\boldsymbol{\kappa}}) = \frac{e^{\jmath \mathbf{p}^{(m,i)} \cdot \overline{\boldsymbol{\kappa}}^{\pm}}}{2\omega\epsilon\, k_z(\overline{\kappa}_x, \overline{\kappa}_y)} \hat{\mathbf{a}}_n(\overline{\boldsymbol{\kappa}}^{\pm}) \cdot \left(\overline{\boldsymbol{\kappa}}^{\pm} \times \overline{\boldsymbol{\kappa}}^{\pm} \times \breve{\boldsymbol{\Phi}}_u^{(i)}(\overline{\boldsymbol{\kappa}}^{\pm})\right) \tag{55}$$

$$\left[\mathbf{G}_{\mathrm{EM}}^{(m,i)}\right]_{u,n} = \left[\mathbf{G}_{\mathrm{EM}}^{(m,i)}\right]_{u,n}(\overline{\boldsymbol{\kappa}}) = -\frac{e^{\jmath \mathbf{p}^{(m,i)} \cdot \overline{\boldsymbol{\kappa}}^{\pm}}}{2\, k_z(\overline{\kappa}_x, \overline{\kappa}_y)} \hat{\mathbf{a}}_n(\overline{\boldsymbol{\kappa}}^{\pm}) \cdot \left(\overline{\boldsymbol{\kappa}}^{\pm} \times \widetilde{\boldsymbol{\Phi}}_u^{(i)}(\overline{\boldsymbol{\kappa}}^{\pm})\right) \tag{56}$$

for $n = 1, 2$, and $u = 1, 2, \ldots, N^{(i)}$, where $\mathbf{p}^{(m,i)} = \left(-p_x^{(i)}, -p_y^{(i)}, z_{\mathrm{o}} - p_z^{(i)}\right)$, and $\overline{\boldsymbol{\kappa}}^{\pm}$ is defined in (85), with $r_z = z_{\mathrm{o}} - p_z^{(i)}$ and $z_{\max} = z_{\min} = 0$. It is worth noticing that the coefficients in (55) and (56) are functions of $\overline{\boldsymbol{\kappa}}$.

C. Coupling Between an EMO and a Harmonic Current

Similarly, closed-form expressions for the coupling coefficients can be obtained when the generic mth EMO is coupled with the harmonic current in (48), that is,

$$\left[\mathbf{G}_{\mathrm{EJ}}^{(m,i)}\right]_{u,n}(\overline{\boldsymbol{\kappa}}) = \frac{e^{\jmath \mathbf{p}^{(m,i)} \cdot \overline{\boldsymbol{\kappa}}^{\pm}}}{2\omega\epsilon\, k_z(\overline{\kappa}_x, \overline{\kappa}_y)} \cdot \left(\underline{\mathsf{R}}^{(m,i)} \cdot \breve{\boldsymbol{\Phi}}_n^{(m)}\left(\mathbf{R}^{(m,i)} \cdot \overline{\boldsymbol{\kappa}}^{\pm}\right)\right)^* \cdot \left(\overline{\boldsymbol{\kappa}}^{\pm} \times \overline{\boldsymbol{\kappa}}^{\pm} \times \hat{\mathbf{a}}\right) \tag{57}$$

$$\left[\mathbf{G}_{\mathrm{EM}}^{(m,i)}\right]_{u,n}(\overline{\boldsymbol{\kappa}}) = -\frac{e^{\jmath \mathbf{p}^{(m,i)} \cdot \overline{\boldsymbol{\kappa}}^{\pm}}}{2\, k_z(\overline{\kappa}_x, \overline{\kappa}_y)} \cdot \left(\underline{\mathsf{R}}^{(m,i)} \cdot \breve{\boldsymbol{\Phi}}_n^{(m)}\left(\mathbf{R}^{(m,i)} \cdot \overline{\boldsymbol{\kappa}}^{\pm}\right)\right)^* \cdot \left(\overline{\boldsymbol{\kappa}}^{\pm} \times \hat{\mathbf{a}}\right) \tag{58}$$

for $u = 1$, where $\mathbf{p}^{(m,i)} = \left(p_x^{(m)}, p_y^{(m)}, p_z^{(m)} - z_{\mathrm{s}}\right)$, and $\overline{\boldsymbol{\kappa}}^{\pm}$ is defined in (85), with $r_z = p_z^{(m)} - z_{\mathrm{s}}$ and $z_{\max} = z_{\min} = 0$. Also in this case the coefficients are functions of $\overline{\boldsymbol{\kappa}}$.

D. Self-Coupling in Surfaces

In this case, $\mathbf{R}^{(m,m)} = \mathbf{I}_3$ and $\mathbf{p} = \mathbf{p}^{(m,m)} = (0, 0, p_z)$, with $p_z = (1 - 2n_{\mathrm{s}})\, \Delta/2$ depending whether side $n_{\mathrm{s}} = 0$ or $n_{\mathrm{s}} = 1$ is considered. The basis functions associated with currents are located at $z = 0$. As a consequence, (51) and (52) read

$$\left[\mathbf{G}_{\mathrm{EJ}}^{(m,m)}\right]_{u,n} = \frac{\pi}{\omega\epsilon(2\pi)^3} \int_{\mathcal{R}^2} \frac{k_{u,n}(\kappa_x, \kappa_y)\, e^{\jmath k_z(\kappa_x, \kappa_y)\Delta/2}}{k_z(\kappa_x, \kappa_y)} \cdot \left(\tilde{\phi}_n^{(m)}(\boldsymbol{\kappa})\right)^* \cdot \left(\tilde{\phi}_u^{(m)}(\boldsymbol{\kappa})\right) d\kappa_x\, d\kappa_y \tag{59}$$

$$\left[\mathbf{G}_{\mathrm{EM}}^{(m,m)}\right]_{u,n} = -\frac{\pi}{(2\pi)^3} \int_{\mathcal{R}^2} \frac{k_{u,n}^{\star}(\kappa_x, \kappa_y)\, e^{\jmath k_z(\kappa_x, \kappa_y)\Delta/2}}{k_z(\kappa_x, \kappa_y)} \cdot \left(\tilde{\phi}_n^{(m)}(\boldsymbol{\kappa})\right)^* \cdot \left(\tilde{\phi}_u^{(m)}(\boldsymbol{\kappa})\right) d\kappa_x\, d\kappa_y \tag{60}$$

where index n refers to the nth current basis function (at $z = 0$), and index u refers to the uth basis function of the EM field on both sides of the surfaces at $p_z = (1 - 2n_{\mathrm{s}})\, \Delta/2$ depending on n_{s}. In addition, $k_{u,n}(\kappa_x, \kappa_y) = -\kappa_y^2 - k_z^2(\kappa_x, \kappa_y)$, $k_{u,n}^{\star}(\kappa_x, \kappa_y) = 0$ when $\hat{\mathbf{a}}_n = \hat{\mathbf{a}}_u = \hat{\mathbf{x}}$, $k_{u,n}(\kappa_x, \kappa_y) = -\kappa_x^2 - k_z^2$, $k_{u,n}^{\star}(\kappa_x, \kappa_y) = 0$ when $\hat{\mathbf{a}}_n = \hat{\mathbf{a}}_u = \hat{\mathbf{y}}$, $k_{u,n} = \kappa_x\, \kappa_y$, $k_{u,n}^{\star}(\kappa_x, \kappa_y) = k_z(\kappa_x, \kappa_y)\, (n_{\mathrm{p}} - u_{\mathrm{p}})(1 - 2n_{\mathrm{s}})$ when $\hat{\mathbf{a}}_n \neq \hat{\mathbf{a}}_u$, with $\hat{\mathbf{a}}_n \in \{\hat{\mathbf{x}}, \hat{\mathbf{y}}\}$ and $\hat{\mathbf{a}}_u \in \{\hat{\mathbf{x}}, \hat{\mathbf{y}}\}$ being the polarization of $\breve{\boldsymbol{\Phi}}_n^{(m)}(\boldsymbol{\kappa})$ and $\breve{\boldsymbol{\Phi}}_u^{(m)}(\boldsymbol{\kappa})$, respectively. When the polarizations are equal (i.e., $n_{\mathrm{p}} = u_{\mathrm{p}}$), $k_{u,n}^{\star}(\kappa_x, \kappa_y) = 0$ and hence $\left[\mathbf{G}_{\mathrm{EM}}^{(m,m)}\right]_{u,n} = 0$. When $n_{\mathrm{p}} \neq u_{\mathrm{p}}$, $n_x = u_x$ and $n_u = u_y$ we have

$$\left[\mathbf{G}_{\mathrm{EM}}^{(m,m)}\right]_{u,n} = -\frac{\pi\, (n_{\mathrm{p}} - u_{\mathrm{p}})(1 - 2n_{\mathrm{s}})\, \delta_{u_x - n_x,\, u_y - n_y}}{(2\pi)^3} \cdot \int_{\mathcal{R}^2} e^{\jmath k_z(\kappa_x, \kappa_y)\Delta/2} \left(\tilde{\phi}_n^{(m)}(\boldsymbol{\kappa})\right)^* \cdot \left(\tilde{\phi}_u^{(m)}(\boldsymbol{\kappa})\right) d\kappa_x\, d\kappa_y. \tag{61}$$

E. Self-Coupling in Large Surfaces

When $L_x, L_y \gg \lambda$, the unitary energy functions $S_n(k; L)$ in (41) composing $\tilde{\phi}_n^{(m)}(\boldsymbol{\kappa})$ tend to zero very quickly around their maximum value compared to the speed of variations of the other terms of the integrating function, therefore, the latter

can be approximated as constant and the integrals (59) and (60) solved, thus obtaining

$$\left[\mathbf{G}_{\mathrm{EJ}}^{(m,m)}\right]_{u,n} \simeq \frac{\delta_{u_x-n_x,\,u_y-n_y}}{2\,\omega\epsilon}\,\frac{k_{u,n}^{(n)}}{k_z^{(n)}}\,e^{\jmath k_z^{(n)}\Delta/2} \tag{62}$$

$$\left[\mathbf{G}_{\mathrm{EM}}^{(m,m)}\right]_{u,n} \simeq -\frac{(n_{\mathrm{p}}-u_{\mathrm{p}})(1-2n_{\mathrm{s}})\,\delta_{u_x-n_x,\,u_y-n_y}}{2}\,e^{\jmath k_z^{(n)}\Delta/2} \tag{63}$$

with $k_x^{(n)} = \frac{2\pi n_x}{L_x}$, $k_y^{(n)} = \frac{2\pi n_y}{L_y}$, $k_z^{(n)} = k_z\left(k_x^{(n)}, k_y^{(n)}\right)$, and $k_{u,n}^{(n)} = k_{u,n}\left(k_x^{(n)}, k_y^{(n)}\right)$. When $L_x, L_y \to \infty$ (62) converges to $-\delta_{u_x-n_x,\,u_y-n_y}\,\eta\,e^{\jmath k_0\Delta/2}/2$. It is worth noticing that in large surfaces, the self-coupling between different modes ($u \neq n$) is approximately equal to zero, i.e., the orthogonality is preserved. Therefore, the only way to couple different modes is through the constitutive equations in (7).

VI. Constitutive Equations for Large Surfaces

In this section, we show some derivation examples of matrix $\mathbf{D}$ in (35), associated with the constitutive equations in (7), for a large surface EMO. Consider the generic mth EMO with surface $\mathcal{S}^{(m)}$. In the following, we omit the superscript m to lighten the notation. To simplify the examples, we consider the isotropic case, then dyadic $\underline{\mathsf{D}}_{\mathrm{w}}$ is of multiplicative type as $\underline{\mathsf{D}}_{\mathrm{w}} = X_{\mathrm{w}}(\mathbf{r})$, with $\mathrm{w} \in \{\mathrm{JE}, \mathrm{JH}, \mathrm{ME}, \mathrm{MH}\}$ and $\mathbf{r} \in \mathcal{S}$ [14]. As for current sources and EM fields, function $X_{\mathrm{w}}(\mathbf{r})$ can be expressed in terms of series expansion

$$X_{\mathrm{w}}(\mathbf{r}) = \sum_{j=1}^{N_x\,N_y} X_{\mathrm{w}_j}\,\phi_j(\mathbf{r})\,e^{-\jmath k_0\,\Delta/2} \tag{64}$$

where $X_{\mathrm{w}_j} = \left\langle X_{\mathrm{w}}(\mathbf{r}), \phi_j(\mathbf{r})\right\rangle$ and $\left\{\phi_j(\mathbf{r})\right\}$ is a (scalar) basis set for $\mathcal{S}$. The exponential term in (64) accounts for the fact that we consider the currents located at $z = 0$, whereas the EM fields are observed on the right/left sides of the surface at $z = \pm\Delta/2$, according to the model described in Sec. IV-C. It follows that matrix $\mathbf{D}_{\mathrm{w}}$ in (35) can be written as $\mathbf{D}_{\mathrm{w}} = \mathrm{diag}\,(\mathbf{X}_{\mathrm{w}}, \mathbf{X}_{\mathrm{w}}, \mathbf{X}_{\mathrm{w}}, \mathbf{X}_{\mathrm{w}})$, where $\mathbf{X}_{\mathrm{w}}$ is a $N_x \times N_y$ matrix whose generic element is given by

$$\begin{aligned}[\mathbf{X}_{\mathrm{w}}]_{u,n} &= \left\langle \underline{\mathsf{D}}_{\mathrm{w}} \cdot \boldsymbol{\Phi}_u(\mathbf{r}), \boldsymbol{\Phi}_n(\mathbf{r})\right\rangle \\ &= \sum_{j=1}^{N_x\,N_y} X_{\mathrm{w}_j}\left\langle \phi_j(\mathbf{r})\cdot\boldsymbol{\phi}_u(\mathbf{r}), \boldsymbol{\phi}_n(\mathbf{r})\right\rangle\end{aligned} \tag{65}$$

for $n, u = 1, 2, \ldots, N_x\,N_y$. In a more compact form, we can write

$$\mathbf{X}_{\mathrm{w}} = \sum_{j=1}^{N_x\,N_y} X_{\mathrm{w}_j}\,\mathbf{H}_j \tag{66}$$

where $\left[\mathbf{H}_j\right]_{n,u} = \left\langle \phi_j(\mathbf{r})\,\boldsymbol{\phi}_u(\mathbf{r}), \boldsymbol{\phi}_n(\mathbf{r})\right\rangle$. In case the basis functions in Sec. IV-C are used, it is

$$\left[\mathbf{H}_j\right]_{n,u} = \frac{1}{\sqrt{L_x\,L_y}}\delta_{j_x+u_x-n_x}\delta_{j_y+u_y-n_y}\,e^{-\jmath k_0\,\Delta/2}. \tag{67}$$

It is evident from (67) that the effect produced by a surface on induced currents as a function of the EM field corresponds to a coupling between different modes depending on the values of coefficients X_{w_j} which characterize the behavior of the surface.

A. Modeling the Equivalent Homogenized Boundary Conditions

We here illustrate how the equivalent homogenized boundary conditions typically used to model metasurfaces can be accounted for in our framework. Specifically, we model the surface as an inhomogeneous sheet of polarizable particles characterized by an electric surface impedance and magnetic surface admittance. This constitutes the homogenized model of the surface where the average electric and magnetic fields induce electric and magnetic currents generating a discontinuity of the EM field between the two sides of the surface [14], [17], [22]. The corresponding boundary conditions are referred to as generalized sheet transition conditions. We consider the case in which the surface imposes an equivalent homogenized boundary condition of the type [16], [22]

$$\begin{aligned}\begin{pmatrix}\mathsf{J}_{\mathrm{s}}(\mathbf{r})\\ \mathsf{M}_{\mathrm{s}}(\mathbf{r})\end{pmatrix} &= \frac{1}{2}\begin{pmatrix}\mathsf{Y}_{\mathrm{JE}}(\mathbf{r}) & \mathsf{Y}_{\mathrm{JH}}(\mathbf{r})\\ \mathsf{Y}_{\mathrm{ME}}(\mathbf{r}) & \mathsf{Y}_{\mathrm{MH}}(\mathbf{r})\end{pmatrix}\cdot\begin{pmatrix}\mathsf{E}_{\mathrm{t}}^{+}(\mathbf{r})+\mathsf{E}_{\mathrm{t}}^{-}(\mathbf{r})\\ \mathsf{H}_{\mathrm{t}}^{+}(\mathbf{r})+\mathsf{H}_{\mathrm{t}}^{-}(\mathbf{r})\end{pmatrix}\\ &= \frac{1}{2}\begin{pmatrix}\mathsf{Y}_{\mathrm{JE}}(\mathbf{r}) & \mathsf{Y}_{\mathrm{JH}}(\mathbf{r})\\ \mathsf{Y}_{\mathrm{ME}}(\mathbf{r}) & \mathsf{Y}_{\mathrm{MH}}(\mathbf{r})\end{pmatrix}\cdot\begin{pmatrix}1 & 1 & 0 & 0\\ 0 & 0 & 1 & 1\end{pmatrix}\begin{pmatrix}\mathsf{E}_{\mathrm{t}}^{+}(\mathbf{r})\\ \mathsf{E}_{\mathrm{t}}^{-}(\mathbf{r})\\ \mathsf{H}_{\mathrm{t}}^{+}(\mathbf{r})\\ \mathsf{H}_{\mathrm{t}}^{-}(\mathbf{r})\end{pmatrix}\end{aligned} \tag{68}$$

where $\mathsf{E}_{\mathrm{t}}^{+}(\mathbf{r})$, $\mathsf{H}_{\mathrm{t}}^{+}(\mathbf{r})$, $\mathsf{E}_{\mathrm{t}}^{-}(\mathbf{r})$, $\mathsf{H}_{\mathrm{t}}^{-}(\mathbf{r})$ are the electric and magnetic tangent fields, respectively, at the right (+) and left (-) sides of the surface, being $\mathsf{Y}_{\mathrm{JE}}(\mathbf{r})$ and $\mathsf{Y}_{\mathrm{MH}}(\mathbf{r})$ the electric sheet admittance and magnetic sheet impedance, respectively. It follows that $X_{\mathrm{w}}(\mathbf{r}) = \mathsf{Y}_{\mathrm{w}}(\mathbf{r})$ with $\mathrm{w} \in \{\mathrm{JE}, \mathrm{JH}, \mathrm{ME}, \mathrm{MH}\}$. In terms of linear algebra formulation, the previous equivalent homogenized boundary conditions read

$$\begin{aligned}\mathbf{b} &= \frac{1}{2}\begin{pmatrix}\mathbf{X}_{\mathrm{JE}} & \mathbf{0}_N & \mathbf{X}_{\mathrm{JH}} & \mathbf{0}_N\\ \mathbf{0}_N & \mathbf{X}_{\mathrm{JE}} & \mathbf{0}_N & \mathbf{X}_{\mathrm{JH}}\\ \mathbf{X}_{\mathrm{ME}} & \mathbf{0}_N & \mathbf{X}_{\mathrm{MH}} & \mathbf{0}_N\\ \mathbf{0}_N & \mathbf{X}_{\mathrm{ME}} & \mathbf{0}_N & \mathbf{X}_{\mathrm{MH}}\end{pmatrix}\begin{pmatrix}\mathbf{I}_{2N} & \mathbf{I}_{2N} & \mathbf{0}_{2N} & \mathbf{0}_{2N}\\ \mathbf{0}_{2N} & \mathbf{0}_{2N} & \mathbf{I}_{2N} & \mathbf{I}_{2N}\end{pmatrix}\\ &\quad\times\begin{pmatrix}\mathbf{e}^{+}\\ \mathbf{e}^{-}\\ \mathbf{h}^{+}\\ \mathbf{h}^{-}\end{pmatrix}\\ &= \mathbf{D}\cdot\mathbf{f}\end{aligned} \tag{69}$$

with $N = N_x\,N_y$, where $\mathbf{e}^{+}$ and $\mathbf{e}^{-}$ represent, respectively, the first and the second group of $2N$ elements of vector $\mathbf{e}$ associated with the two sides of the surface. The same meaning holds for $\mathbf{h}^{+}$ and $\mathbf{h}^{-}$.

B. Impedance Sheet

For a metasurface backed by a ground plane, the boundary conditions can be expressed in terms of an impenetrable equivalent impedance or admittance which relates the average tangent electric and magnetic fields on top of the surface as $\mathsf{E}_{\mathrm{t}}(\mathbf{r}) = \mathsf{Z}(\mathbf{r})\,\hat{\mathbf{z}}\times\mathsf{H}_{\mathrm{t}}(\mathbf{r}) = \mathsf{Z}(\mathbf{r})\,\mathsf{J}_{\mathrm{s}}(\mathbf{r})$ [18]. In this case, $\mathsf{J}_{\mathrm{s}}(\mathbf{r}) = \mathsf{Y}_{\mathrm{JE}}(\mathbf{r})\,\mathsf{E}_{\mathrm{t}}(\mathbf{r})$, $\mathsf{M}_{\mathrm{s}}(\mathbf{r}) = 0$, with $\mathsf{Y}_{\mathrm{JE}}(\mathbf{r}) = \mathsf{Z}^{-1}(\mathbf{r})$. As a consequence, matrix $\mathbf{D}$ in (69) simplifies into

$$\mathbf{D} = \begin{pmatrix}\mathbf{X}_{\mathrm{JE}} & \mathbf{0}_N & \mathbf{0}_N & \mathbf{0}_N\\ \mathbf{0}_N & \mathbf{X}_{\mathrm{JE}} & \mathbf{0}_N & \mathbf{0}_N\\ \mathbf{0}_N & \mathbf{0}_N & \mathbf{0}_N & \mathbf{0}_N\\ \mathbf{0}_N & \mathbf{0}_N & \mathbf{0}_N & \mathbf{0}_N\end{pmatrix}\begin{pmatrix}\mathbf{I}_{2N} & \mathbf{0}_{2N} & \mathbf{0}_{2N} & \mathbf{0}_{2N}\\ \mathbf{0}_{2N} & \mathbf{0}_{2N} & \mathbf{0}_{2N} & \mathbf{0}_{2N}\end{pmatrix}. \tag{70}$$

VII. EM Transfer Function and IT Channel Matrix

A. EM Transfer Function

We are now in the position of deriving the relationship between the linear algebra method illustrated in Sec. III and the system EM transfer function defined in Sec. II-D. It is customary in the literature to define the EM system transfer function or channel transfer function, namely $\underline{\widetilde{\mathcal{H}}}(\kappa_x,\kappa_y,\overline{\kappa}_x,\overline{\kappa}_y;z_s,z_o)$, with reference to a source in the $x-y$ plane at $z=z_s$, where the impressed (real or equivalent) currents $\mathsf{J}_{imp}(x,y;z_s)$ are supposed to lay, and an $x-y$ observation plane at $z=z_o$ where the electric field $\widetilde{\mathsf{E}}(\kappa_x,\kappa_y;z_o)$ is observed [23], [24], [25], [26]. For example, this could be the plane where a receiving antenna array or a surface is located. It follows that

$$\begin{aligned}\widetilde{\mathsf{E}}(\kappa_x,\kappa_y;z_o)&=\frac{1}{2\pi}\int\widetilde{\mathsf{E}}(\boldsymbol{\kappa})\,e^{\jmath\kappa_z z_o}\,d\kappa_z\\&=\int_{\mathcal{R}^2}\underline{\widetilde{\mathcal{H}}}(\kappa_x,\kappa_y,k_x,k_y;z_s,z_o)\\&\quad\widetilde{\mathsf{J}}_{imp}(k_x,k_y;z_s)\,dk_x\,dk_y\end{aligned}\tag{71}$$

where

$$\begin{aligned}\underline{\widetilde{\mathcal{H}}}(\kappa_x,\kappa_y,\overline{\kappa}_x,\overline{\kappa}_y;z_s,z_o)&=\frac{1}{(2\pi)^2}\int_{\mathcal{R}^2}\underline{\widetilde{\mathcal{H}}}_{EJ}(\boldsymbol{\kappa},\overline{\boldsymbol{\kappa}})\\&\quad\cdot e^{-\jmath\kappa_z z_s}e^{\jmath\overline{\kappa}_z z_o}d\kappa_z\,\overline{\kappa}_z.\end{aligned}\tag{72}$$

The component $\widetilde{\mathcal{H}}^{(xx)}(\kappa_x,\kappa_y,\overline{\kappa}_x,\overline{\kappa}_y;z_s,z_o)$ of (72) gives the system response observed on the plane $z=z_o$ at the 2D wavenumber (κ_x,κ_y) and polarization $\hat{\mathbf{a}}_x$ when solicited by the harmonic current $\widetilde{\mathsf{J}}_{imp}(\boldsymbol{\kappa})=\hat{\mathbf{a}}_x(2\pi)^2\delta(\kappa_x-\overline{\kappa}_x)\,\delta(\kappa_y-\overline{\kappa}_y)\,e^{-\jmath\kappa_z z_s}$ located on the plane $z=z_s$. Note that (72) is a vector transfer function, whereas the treatment in [23], [24], and [25] considers scalar fields.

Now, suppose one is interested in finding, for example, the xx component $\widetilde{\mathcal{H}}^{(xx)}(\cdot)$ of the EM transfer function in (72). To this purpose, we add in the system two virtual EMOs whose indexes are, respectively, 1 and M, with $\mathbf{D}^{(1)}=\mathbf{D}^{(M)}=0$. The first EMO is responsible for the impinging elementary harmonic electric current in (48) with wavenumber $\overline{\boldsymbol{\kappa}}$, whereas the Mth EMO is the virtual plane-wave EMO, with wavenumber $\boldsymbol{\kappa}$, given by (46). Therefore, the number of physical EMOs is $M-2$ and they may have any arbitrary position and orientation. The general problem is to find the algebraic relationship between $\mathbf{f}^{(M)}$ and $\mathbf{a}^{(1)}$ in (40), where the coefficients in matrices $\mathbf{G}^{(M,i)}$, for $i=2,3,\ldots,M-1$, are given by (55) and (56), whereas the coefficients of $\mathbf{G}^{(m,1)}$, for $m=2,3,\ldots,M$, are given by (57) and (58). Considering only the first component of $\mathbf{e}^{(M)}$ in $\mathbf{f}^{(M)}$ (that related to the x polarization), it is

$$\widetilde{\mathcal{H}}^{(xx)}(\kappa_x,\kappa_y,\overline{\kappa}_x,\overline{\kappa}_y;z_s,z_o)=\left[\mathbf{e}^{(M)}(\boldsymbol{\kappa},\overline{\boldsymbol{\kappa}})\right]_{1,1}\tag{73}$$

where vector $\mathbf{e}^{(M)}(\boldsymbol{\kappa},\overline{\boldsymbol{\kappa}})$ is derived by setting $\mathbf{a}^{(1)}=1$, and we made explicit the dependence of $\mathbf{e}^{(M)}$ on the wavenumbers $\overline{\boldsymbol{\kappa}}$ and $\boldsymbol{\kappa}$ of the impinging elementary harmonic electric current and the observed wavenumber, respectively. A similar approach can be applied to the other polarizations. In Sec. VIII, we will illustrate some explicit examples of calculation of the EM transfer function (73).

B. IT Channel Matrix and Antenna DoF

In Sec. II-E, we have seen that the IT channel matrix depends on the antenna's impedance matrix $\mathbf{Z}_T$ and the trasnimpedance matrix $\mathbf{Z}_C$. We want to find the relationship with the previous framework and use it to investigate the fundamental limits of antennas from the IT perspective.

1) Antenna Impedance and IT Channel Matrix: Let us consider an EMO representing a generic P-port transmitting antenna, where we drop the index m for convenience. As mentioned in Sec. II-E, we can replace the antenna structure with an equivalent impressed current $\mathsf{J}(\mathbf{r})=\sum_n a_{J\,n}\boldsymbol{\Phi}_n(\mathbf{r})$ defined on the antenna's surface $\mathcal{S}$, which radiates in free space and can be decomposed using the basis set $\{\boldsymbol{\Phi}_n(\mathbf{r})\}_{n=1}^N$ defined on $\mathcal{S}$. Since $\mathsf{J}(\mathbf{r})$ is a linear function of the currents $\mathbf{i}$ at the ports (defined in Sec. II-E), we can write $\mathbf{a}_J=\mathbf{T}\cdot\mathbf{i}$, where the matrix $\mathbf{T}$ has elements $[\mathbf{T}]_{n,i}=\langle\mathsf{T}(\mathbf{r};\mathbf{z}_i),\boldsymbol{\Phi}_n(\mathbf{r})\rangle$. Here, $\mathbf{z}_i$ is a zero vector except for the ith element, which is equal to one, for $n=1,2,\ldots,N$, and $i=1,2,\ldots,P$. The power radiated by the antenna can be computed by solving the following expression [38, eqn. (8)]

$$\begin{aligned}P_{rad}&=-\frac{1}{2}\mathbb{E}\left\{\int_{\mathcal{V}}\Re\left\{\mathsf{E}(\mathbf{r})\cdot\mathsf{J}^*(\mathbf{r})\right\}\,d\mathbf{r}\right\}\\&=-\frac{1}{2}\mathbb{E}\left\{\Re\left\{\langle\mathsf{E}_t(\mathbf{r}),\mathsf{J}(\mathbf{r})\rangle\right\}\right\}\\&=-\frac{1}{2}\mathbb{E}\left\{\Re\left\{\left\langle\underline{\mathsf{G}}_{EJ}\,\mathsf{J}(\mathbf{r}),\mathsf{J}(\mathbf{r})\right\rangle\right\}\right\}\end{aligned}\tag{74}$$

where $\mathcal{V}$ is the volume in which the current flows. In our case, being the equivalent current $\mathsf{J}(\mathbf{r})$ defined on the EMO's surface $\mathcal{S}$, then $\mathcal{V}=\mathcal{S}$. Denote with $C_{n,u}$ twice the component of (74) obtained by setting $\boldsymbol{\Phi}_n(\mathbf{r})$ and $\boldsymbol{\Phi}_u(\mathbf{s})$ as current terms of the right-hand side inner product in (74). Using (59), $C_{n,u}$ is given by

$$C_{n,u}=-\Re\left\{\left\langle\underline{\mathsf{G}}_{EJ}\,\boldsymbol{\Phi}_n(\mathbf{r}),\boldsymbol{\Phi}_u(\mathbf{r})\right\rangle\right\}=-\Re\left\{[\mathbf{G}_{EJ}]_{u,n}\right\}.\tag{75}$$

As a consequence, by defining the coupling matrix $[\mathbf{C}_T]_{n,u}=C_{n,u}$, for $n,u=1,2,\ldots,N$, (74) can be rewritten as $P_{rad}=\frac{1}{2}\mathbb{E}\left\{\mathbf{a}_J{}^H\mathbf{C}_T\,\mathbf{a}_J\right\}$, which is formally equivalent to the expression of the transmitted power $P_T=\frac{1}{2}\mathbb{E}\left\{\mathbf{i}^H\Re\{\mathbf{Z}_T\}\,\mathbf{i}\right\}$ computed at the input ports. Because of the law of conservation of the energy, $P_T=P_{rad}$ and hence it is $\Re\{\mathbf{Z}_T\}=\mathbf{T}^H\mathbf{C}_T\mathbf{T}$, which indicates that (75) is a general approach to compute the real part of the impedance matrix $\mathbf{Z}_T$ which impacts the IT channel matrix $\mathbf{H}$ in (18).

Regarding the transimpedance matrix $\mathbf{Z}_C$, supposing for simplicity that the EMO with $m=1$ represents the transmitting antenna and the EMO with $m=M$ the receiving antenna, it follows that $\mathbf{Z}_C$ corresponds to the matrix that relates the component $\mathbf{e}^{(M)}$ of $\mathbf{f}^{(M)}$ and $\mathbf{a}^{(1)}=[\mathbf{a}_J,\mathbf{0}_N]^T$. Depending on the scenario, such a relation can be found solving the matrix equations in (40), in a similar way followed to derive the EM transfer function in Sec. VII-A.

2) DoF of an Antenna: The capacity of the IT channel depends on the rank of matrix $\mathbf{H}$ in (18), which in turn is limited by $\min(r_T,r_C,r_R)$, where $r_T=\text{rank}(\Re\{\mathbf{Z}_T\})$, $r_C=\text{rank}(\mathbf{Z}_C)$, and $r_R=\text{rank}(\Re\{\mathbf{Z}_R\})$. While r_C depends on the overall propagation environment, r_T and r_R are limited by the antennas' geometry and the number of ports that, in certain scenarios (e.g., multi-user systems), might represent

the bottleneck of the system capacity. Therefore, it is of interest to understand what are the fundamental limits on r_{T}, i.e., the DoF of the antenna.

While the previous result depends on the specific structure of the antenna accounted for by matrix $\mathbf{T}$, the same approach above can be used to abstract from the specific implementation of the antenna and the actual number of ports P and used to identify the theoretical limits of the antenna starting from the geometry of its surface $\mathcal{S}$. To elaborate, imagine now the antenna is driven by the currents $\mathbf{i}$ and voltages $\mathbf{v}$ at the N imaginary ports pulled out from a box that represents the inside of the antenna, each of them associated with each of the N modes in which $\mathsf{J}(\mathbf{r})$ can be decomposed using the basis set $\{\mathbf{\Phi}_n(\mathbf{r})\}$. In this case it is $\mathbf{T} = \mathbf{T}^{(\mathrm{th})} = \mathrm{diag}\,(\mathbf{q})$, where $q_n = \sqrt{L_x/L_y}$, for $n_{\mathrm{p}} = 0$ (x polarization), and $q_n = \sqrt{L_y/L_x}$, for $n_{\mathrm{p}} = 1$ (y polarization), to properly map currents to current densities of a surface. Denote with $\mathbf{Z}_{\mathrm{T}}^{(\mathrm{th})}$ the impedance matrix of the N ports so that $\mathbf{v} = \mathbf{Z}_{\mathrm{T}}^{(\mathrm{th})}\,\mathbf{i}$, where $\Re\left\{\mathbf{Z}_{\mathrm{T}}^{(\mathrm{th})}\right\} = \left(\mathbf{T}^{\mathrm{th}}\right)^{T}\,\mathbf{C}_{\mathrm{T}}\mathbf{T}^{(\mathrm{th})}$, with $\mathbf{C}_{\mathrm{T}}$ given by (75). Note that $\mathbf{Z}_{\mathrm{T}}^{(\mathrm{th})}$ depends only on the geometry of the surface $\mathcal{S}$ and accounts for modes coupling (e.g., between different polarizations). It is worth noticing that now $r_{\mathrm{T}} = \mathrm{rank}\left(\Re\left\{\mathbf{Z}_{\mathrm{T}}^{(\mathrm{th})}\right\}\right) = \mathrm{rank}\,(\mathbf{C}_{\mathrm{T}})$, which represents the number of virtual ports necessary to achieve the maximum flexibility in current generation for a given antenna shape $\mathcal{S}$. Specifically, it can be seen as a theoretical upper bound on the actual number P of ports constituting the antenna, whose number is technology-dependent. If $P \leq r_{\mathrm{T}}$, then P might become the bottleneck of the system capacity through matrix $\mathbf{T}$ (technology bottleneck). On the other hand, considering $P > r_{\mathrm{T}}$ would not bring any advantage in terms of flexibility. An example of how such limits can be derived for a LIS will be given in Sec. VIII-C.

VIII. Examples

In this section, we propose two examples of the derivation of the EM transfer function of a reflecting surface and the optimization of a RIS, and one example showing the application of the proposed framework to derive the fundamental limits on the DoF of a large surface antenna.

A. Transfer Function of a Finite Surface With Constant Impedance

Suppose we want to find the transfer function of a generic EMO, numbered with index 2, characterized by a given constitutive matrix $\mathbf{D}^{(2)}$. Here it is $M = 3$. The observation and source planes are placed at $z_{\mathrm{o}} = z_{\mathrm{s}} = 0$ and the surface at position $\mathbf{p} = (0, 0, p_z)$ with $p_z > 0$. By combining (40) for $m = 2$ and $m = M = 3$, it is

$$\begin{aligned}\mathbf{f}^{(M)}(\boldsymbol{\kappa}, \overline{\boldsymbol{\kappa}}) =& \mathbf{f}^{(3)}(\boldsymbol{\kappa}, \overline{\boldsymbol{\kappa}}) \\ =& \mathbf{G}^{(3,2)}(\boldsymbol{\kappa})\,\mathbf{D}^{(2)}\left(\mathbf{I} - \mathbf{G}^{(2,2)}\,\mathbf{D}^{(2)}\right)^{-1}\,\mathbf{G}^{(2,1)}(\overline{\boldsymbol{\kappa}})\,\mathbf{a}^{(1)}.\end{aligned} \tag{76}$$

As an example, let the surface of the EMO be characterized by a constant admittance across the surface $\mathcal{S}^{(2)}$ of size $L_{\mathrm{x}} \times L_{\mathrm{y}}$, i.e., $\Upsilon(\mathbf{r}) = Y = 1/Z$, for $\mathbf{r} \in \mathcal{S}^{(2)}$, being Z the surface's impedance. From (65), it follows that $X_{\mathrm{JE}_j} = \left\langle \Upsilon(\mathbf{r}), \phi_j(\mathbf{r}) \right\rangle = Y\sqrt{L_{\mathrm{x}}\,L_{\mathrm{y}}}\,\delta_{j-n_0}$, where $n_0 = (N_x - 1)/2 + N_x(N_y - 1)/2 + 1$ is the coefficient of the series expansion (64) corresponding to the basis function for $n_x = n_y = 0$ (continuous component). Therefore, only one term in (64) is different from zero and matrix $\mathbf{X}_{\mathrm{JE}}$ is given by $\mathbf{X}_{\mathrm{JE}} = Y\sqrt{L_{\mathrm{x}}\,L_{\mathrm{y}}}\mathbf{H}_{n_0}$. By letting $\Delta \to 0$, it holds

$$\mathbf{D}^{(2)} = Y\begin{pmatrix} \mathbf{I}_N & \mathbf{0}_N & \mathbf{0}_N & \mathbf{0}_N & \mathbf{0}_N & \mathbf{0}_N & \mathbf{0}_N & \mathbf{0}_N \\ \mathbf{0}_N & \mathbf{I}_N & \mathbf{0}_N & \mathbf{0}_N & \mathbf{0}_N & \mathbf{0}_N & \mathbf{0}_N & \mathbf{0}_N \\ \mathbf{0}_N & \mathbf{0}_N & \mathbf{0}_N & \mathbf{0}_N & \mathbf{0}_N & \mathbf{0}_N & \mathbf{0}_N & \mathbf{0}_N \\ \mathbf{0}_N & \mathbf{0}_N & \mathbf{0}_N & \mathbf{0}_N & \mathbf{0}_N & \mathbf{0}_N & \mathbf{0}_N & \mathbf{0}_N \end{pmatrix}. \tag{77}$$

After a few tedious but straightforward matrix computations, it results

$$\begin{aligned}&\widetilde{\mathcal{H}}^{(xx)}(\kappa_x, \kappa_y, \overline{\kappa}_x, \overline{\kappa}_y; 0, 0) \\ &= \left[\mathbf{e}^{(M)}(\boldsymbol{\kappa}, \overline{\boldsymbol{\kappa}})\right]_1 \\ &= \frac{\eta^2\,L_{\mathrm{x}}\,L_{\mathrm{y}}\,e^{\jmath p_z(k_z(\kappa_x,\kappa_y)+k_z(\overline{\kappa}_x,\overline{\kappa}_y))}}{4} \\ &\quad\cdot\sum_{n_x=1}^{N_x}\sum_{n_y=1}^{N_y} R_n\,\mathrm{Sinc}\left(\frac{\kappa_x L_{\mathrm{x}}}{2\pi} - n_x\right)\mathrm{Sinc}\left(\frac{\kappa_y L_{\mathrm{y}}}{2\pi} - n_y\right) \\ &\qquad\cdot\mathrm{Sinc}\left(\frac{\overline{\kappa}_x L_{\mathrm{x}}}{2\pi} - n_x\right)\mathrm{Sinc}\left(\frac{\overline{\kappa}_y L_{\mathrm{y}}}{2\pi} - n_y\right)\end{aligned} \tag{78}$$

where $R_n = Y\Big/\left(1 + \frac{Y\,\eta\,k_z^{(n)}}{2\,k_0\,k_{n,n}^{(n)}}\right)$, $\eta = k_0/(\omega\,\epsilon)$, and we have exploited the following relationship $\hat{\mathbf{x}}\cdot(\boldsymbol{\kappa}\times\boldsymbol{\kappa}\times\hat{\mathbf{x}}) = k_z(\kappa_x, \kappa_y)$. From (78), it can be evinced that each mode is, in general, subjected to a different reflecting coefficient R_n.

It is interesting to investigate the particular case where $Z = 0$, for which $R_n = 2/\eta$. Letting $N_x, N_y \to \infty$ and considering that $\sum_n \mathrm{Sinc}\,(A - n)\,\mathrm{Sinc}\,(B - n) = \mathrm{Sinc}\,(A - B)$, (78) simplifies into

$$\begin{aligned}&\widetilde{\mathcal{H}}^{(xx)}(\kappa_x, \kappa_y, \overline{\kappa}_x, \overline{\kappa}_y; 0, 0) \\ &\quad= \frac{\eta\,L_{\mathrm{x}}\,L_{\mathrm{y}}\,e^{\jmath p_z(k_z(\kappa_x,\kappa_y)+k_z(\overline{\kappa}_x,\overline{\kappa}_y))}}{2} \\ &\qquad\cdot\mathrm{Sinc}\left(\frac{L_{\mathrm{x}}(\kappa_x - \overline{\kappa}_x)}{2\pi}\right)\mathrm{Sinc}\left(\frac{L_{\mathrm{y}}(\kappa_y - \overline{\kappa}_y)}{2\pi}\right).\end{aligned} \tag{79}$$

It is worth noticing that (79) is proportional to the result found in [20] related to the evaluation of the response of a finite-size rectangular perfect electric conductor. By letting $L_{\mathrm{x}}, L_{\mathrm{y}} \to +\infty$ and considering that $\lim_{x\to+\infty} x\,\mathrm{Sinc}\,(a\,x) = \delta(a)$, we obtain

$$\begin{aligned}&\widetilde{\mathcal{H}}^{(xx)}(\kappa_x, \kappa_y, \overline{\kappa}_x, \overline{\kappa}_y; 0, 0) \\ &\quad= \frac{\eta\delta(\kappa_x - \overline{\kappa}_x)\delta(\kappa_y - \overline{\kappa}_y)e^{\jmath 2\,p_z k_z(\kappa_x,\kappa_y)}}{2}\end{aligned} \tag{80}$$

that is, the transfer function of an infinite size surface, recently derived in [26], which represents a particular case of our more general formula (78). Specifically, (80) indicates that the reflected field can be obtained equivalently by considering a virtual source at a distance $2\,p_z$. This is nothing else than the *image theorem* saying that the reflection operated by a (large) perfect conductor is equivalent to a mirror image of the source [29].

B. RIS Optimization

In the next example, we consider a RIS made of an inhomogeneous sheet of polarizable particles characterized by an electric surface impedance and magnetic surface admittance according to the equivalent homogenized boundary condition in (68). Suppose that the RIS has dimension $L_x = 1.06\,\text{m}$, $L_y = 1.06\,\text{m}$, and whose purpose is to reflect, with a reflection angle $\theta_r = 22°$ along the $x-z$ plane (i.e., $\kappa_x^{(r)} = k_0 \sin(\theta_r)$, $\kappa_y^{(r)} = 0$), an impinging EM field with wavelength $\lambda = 10\,\text{cm}$ and incident angle $\theta_i = 0$ ($\overline{\kappa}_x^{(i)} = \overline{\kappa}_y^{(i)} = 0$). Three different RIS design methods are considered: *Method 1)* Conventional approach where the surface is characterized by a periodic admittance $\mathsf{Y}_{JE}(\mathbf{r}) = \frac{1}{\eta}\sin\left(\kappa_x^{(r)} r_x\right)$, $\mathsf{Y}_{MH}(\mathbf{r}) = \eta^2 \mathsf{Y}_{JE}(\mathbf{r})$, and $\mathsf{Y}_{ME}(\mathbf{r}) = \mathsf{Y}_{JH}(\mathbf{r}) = 0$ [16]. Matrix $\mathbf{D}$ is designed as consequence using (64), (66), (67), and (69); *Method 2)* Matrix $\mathbf{D}$ is obtained as a numerical solution of the following constrained nonlinear optimization problem:

$$\max_{\mathbf{D}} \left| \widetilde{\mathcal{H}}^{(xx)}\left(\kappa_x^{(r)}, \kappa_y^{(r)}, \overline{\kappa}_x^{(i)}, \overline{\kappa}_y^{(i)}; 0, 0\right)\right| \quad \text{s.t. } P_{\text{rad}} = \text{constant} \tag{81}$$

with $\widetilde{\mathcal{H}}^{(xx)}\left(\kappa_x^{(r)}, \kappa_y^{(r)}, \overline{\kappa}_x^{(i)}, \overline{\kappa}_y^{(i)}; 0, 0\right)$ computed using (73) and (76); *Method 3)* Matrix $\mathbf{D}$ is evaluated analytically by solving the following equation extracted from (76) $\mathbf{D}^{(2)}\left(\mathbf{I} - \mathbf{G}^{(2,2)}\mathbf{D}^{(2)}\right)^{-1} = \mathbf{R}_d$, from which $\mathbf{D}^{(2)} = \left(\mathbf{I} + \mathbf{R}_d\,\mathbf{G}^{(2,2)}\right)^{-1}\mathbf{R}_d$, where $\mathbf{R}_d$ is the desired response of the RIS, i.e., how received modes should be mapped into reflected modes. In particular, $\mathbf{R}_d$ is a zero matrix with only one element different from zero in the position where the input mode, corresponding to the impinging wave $\overline{\kappa}_x^{(i)} = 0$, is mapped to the output mode corresponding (or close) to $\kappa_x^{(r)}$. Since we consider only the reflection along the $x-z$ plane, the following numerical results were obtained by setting $N_x = 25$ and $N_y = 1$.

In Fig. 4(a), the amplitude of the RIS transfer function $\widetilde{\mathcal{H}}^{(xx)}(\kappa_x, 0, \overline{\kappa}_x, ; 0, 0)$ for a RIS designed according to Method 1 is reported. The wavenumbers are normalized with respect to k_0. As expected, the transfer function provides some gain at $\overline{\kappa}_x = 0$ and $\kappa_x = \kappa_x^{(r)}$ $\left(\kappa_x^{(r)}/k_0 = 0.38\right)$, which means that the incident wave is correctly reflected towards θ_r. However, as it can be noticed, the periodic nature of the surface generates parasitic reflections in unwanted directions, as predicted by Floquet's theory whose evaluation typically requires EM-level simulations [10], [15]. When the RIS is used in a multi-user wireless system, such parasitic reflections may generate interference to users located at different angles with respect to that of the target user. To reduce the interference, Method 2 can be adopted within our framework to strengthen the signal reflected in the right direction, thus reducing the intensity of the Floquet modes, as it can be noticed in Fig. 4(b) obtained using Method 2. In any case, even if the Floquet modes are mitigated, the obtained EM transfer function might still generate significant interference. In fact, the off-diagonal behavior of the plot indicates that any other EM wave arriving with a different incident angle, i.e., with $\overline{\kappa}_x \neq 0$, would be reflected as well as that with $\overline{\kappa}_x = 0$. In other words, the RIS acts as an anomalous mirror for all the signal sources present in the environment by generating additional interference in uncontrolled directions. This aspect has been often overlooked in the literature. Although the optimization problem in (81) aims to eliminate any spurious reflection, the specific structure of matrix $\mathbf{D}$, being a linear combination of off-diagonal-like matrices $\mathbf{H}_j$ in (67), introduces constraints on its design flexibility. This limitation in the structure of matrix $\mathbf{D}$ arises as a consequence of the local boundary conditions (68) and might hinder the achievement of the desired outcome. Such a constraint is not intrinsically present when using Method 3 according to which $\mathbf{D}$ can take any form depending on the desired modes conversion behavior $\mathbf{R}_d$. The corresponding EM transfer function, depicted in Fig. 4(c), clearly reflects towards θ_r only those waves arriving with an incident angle $\theta_i = 0$, whereas any other wave with different angle is not reflected, thus avoiding the generation of interference caused by Floquet modes and/or other EM sources. From the practical point of

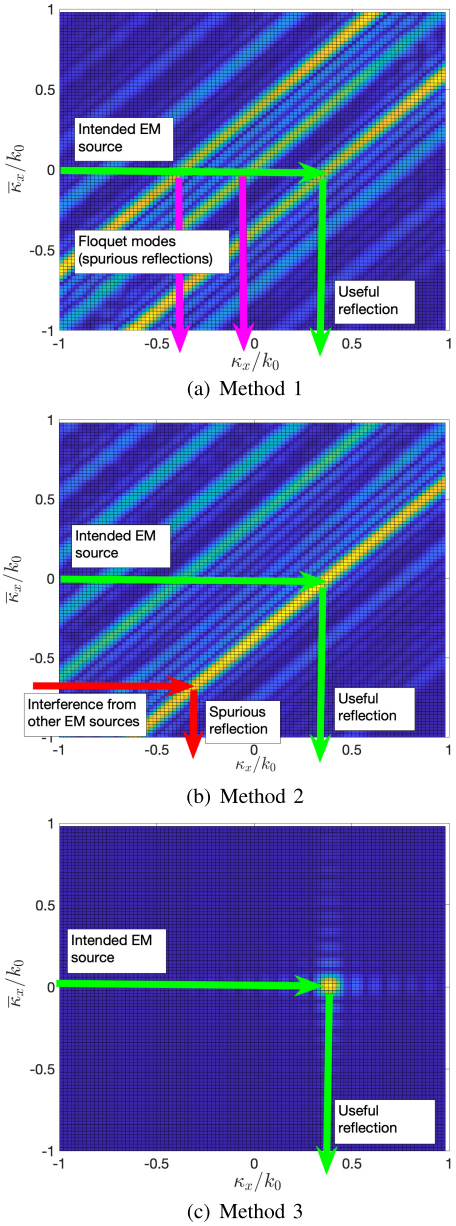

Fig. 4. Amplitude of the RIS' transfer function $\widetilde{\mathcal{H}}^{(xx)}(\kappa_x, 0, \overline{\kappa}_x; 0, 0)$.

view, an unconstrained matrix $\mathbf{D}$ requires more complex EM structures imposing linear constraints at the global surface level [39]. Such structures, i.e., linear EMOs, act as *universal mode converters* [7].

C. Fundamental Limits on the DoF of a LIS

Starting from the approach proposed in Sec. VII-B, here we compute the theoretical limits on the DoF of a large planar thin surface antenna through the computation of the coupling matrix $\mathbf{C}_\mathrm{T}$ in (75). For large surfaces, the coefficient $[\mathbf{G}_\mathrm{EJ}]_{u,n}$ in (75) can be well approximated using (62) with $\Delta = 0$. Therefore, the elements of the coupling matrix $\mathbf{C}_\mathrm{T}$ are

$$C_{n,u} \simeq \frac{\eta}{2}\delta_{u_x-n_x,\,u_y-n_y} \cdot \frac{\delta_{n_\mathrm{p}-u_\mathrm{p}}\left(1-\frac{\lambda^2 n_x^2}{L_x^2}\delta_{n_\mathrm{p}}-\frac{\lambda^2 n_y^2}{L_y^2}\delta_{n_\mathrm{p}-1}\right)-\frac{\lambda^2 n_x n_y}{L_x L_y}\delta_{n_\mathrm{p}+u_\mathrm{p}-1}}{\sqrt{1-\frac{\lambda^2 n_x^2}{L_x^2}-\frac{\lambda^2 n_y^2}{L_y^2}}} \tag{82}$$

when the condition $C_1 : \left\{\frac{\lambda^2 n_x^2}{L_x^2}+\frac{\lambda^2 n_y^2}{L_y^2}<1\right\}$ is satisfied and zero otherwise. For notation convenience, we made use of the mapping introduced in Sec. IV between n, n_x, n_y and n_p.

From the analysis of the coupling matrix $\mathbf{C}_\mathrm{T} = [C_{n,u}]$ in (82) interesting considerations can be derived. To ease the discussion, let us consider a square surface of size $L_x = L_y = L$. The rank $r_\mathrm{T} = \mathrm{rank}\,(\mathbf{C}_\mathrm{T})$ is bounded by twice (2 polarizations) the number of combinations of n_x and n_y that satisfy condition C_1, approximately $r_\mathrm{T} \leq 2\pi\frac{L^2}{\lambda^2}$. Interestingly, a conventional planar array with $\lambda/2$ spaced elements of the same size has $(2L/\lambda)^2$ ports per polarization, then $P = 8\frac{L^2}{\lambda^2}$ ports. Since r_T represents the theoretical upper bound on the DoF, this means that the actual DoF of an P-port planar array is not equal to P but it cannot be larger than $\pi P/4$, i.e., 0.78 P. Compared with the DoF of a spherical array of diameter L given by $\frac{2\pi^2 L^2}{\lambda^2}$ [23], the loss in terms of DoF using a planar surface with respect to a spherical array is equal to π.

IX. Conclusion

In this paper, we have presented a comprehensive and physically consistent framework for characterizing and designing programmable EM environments as a linear graph described by matrix operators. This framework permits the determination of both the EM transfer function of the system and the channel matrix used in IT accounting for the constraints posed by the antenna ports. This description can be used both in theoretical analysis or integrated into system-level simulators without necessitating EM-level simulations that are typically challenging to incorporate into system-level or ray-tracing tools. Various examples have been provided, showcasing its application to the characterization and optimization of RISs. Additionally, the framework has been employed to establish the fundamental limits of the DoF available in LISs antennas. In future works, we aim to extend this framework to include stochastic modeling, enabling a more comprehensive and versatile approach to address varying scenarios and real-world conditions.

Appendix

Consider a source $\mathsf{A}(\mathbf{r})$, whose Fourier transform $\widetilde{\mathsf{A}}(\boldsymbol{\kappa})$ does not exhibit singularities, enclosed within the finite domain $\mathcal{D}$ such that $\mathsf{A}(\mathbf{r}) = 0$, $\forall \mathbf{r} = (r_x, r_y, r_z) \notin \mathcal{D}$. Denote with $z_\mathrm{min} = \min\left(r_z : (r_x, r_y, r_z) \in \mathcal{D}, \forall r_x, r_y\right)$ and with $z_\mathrm{max} = \max\left(r_z : (r_x, r_y, r_z) \in \mathcal{D},\ \forall r_x, r_y\right)$. Suppose the purpose is to compute the inverse Fourier transform of $\widetilde{G}_0(\boldsymbol{\kappa})\,\widetilde{\mathsf{A}}(\boldsymbol{\kappa})$ at location $\mathbf{r}$, with $r_z > z_\mathrm{max}$ or $r_z < z_\mathrm{min}$. Unfortunately, $\widetilde{G}_0(\boldsymbol{\kappa})$ in (11) presents a singularity when $|\boldsymbol{\kappa}| = k_0$, i.e., the condition an EM plane wave must satisfy. If we consider the integration over κ_z to be a contour integration with the contour completed at infinity, then the Cauchy's integral theorem has the effect of enforcing the condition $|\boldsymbol{\kappa}| = k_0$ and hence the well-known more convenient representation of the inverse Fourier transform can be found [32, Ch. 3]

$$\int_{\mathcal{R}^3} \widetilde{G}_0(\boldsymbol{\kappa})\,\widetilde{\mathsf{A}}(\boldsymbol{\kappa})\,e^{\jmath\boldsymbol{\kappa}\cdot\mathbf{r}}\,d^3\boldsymbol{\kappa} = -\jmath\,\pi\int_{\mathcal{R}^2}\frac{\widetilde{\mathsf{A}}(\boldsymbol{\kappa}^\pm)}{k_z(\kappa_x,\kappa_y)}\,e^{\jmath\boldsymbol{\kappa}^\pm\cdot\mathbf{r}}\,d\kappa_x d\kappa_y \tag{83}$$

where

$$k_z = k_z(\kappa_x,\kappa_y) = \begin{cases}\sqrt{k_0^2-\kappa_x^2-\kappa_y^2} & (\kappa_x,\kappa_y)\in\mathcal{P}\\ \jmath\sqrt{\kappa_x^2+\kappa_y^2-k_0^2} & (\kappa_x,\kappa_y)\notin\mathcal{P}\end{cases} \tag{84}$$

$$\boldsymbol{\kappa}^\pm = \begin{cases}(\kappa_x,\kappa_y,k_z) & r_z > z_\mathrm{max}\\ (\kappa_x,\kappa_y,-k_z) & r_z < z_\mathrm{min}\end{cases}. \tag{85}$$

and $\mathcal{P} = \left\{(\kappa_x,\kappa_y)\in\mathbb{R}^2 : \kappa_x^2+\kappa_y^2 \leq k_0^2\right\}$. When $(\kappa_x,\kappa_y)\in\mathcal{P}$, k_z is real and propagation happens. Instead, when $(\kappa_x,\kappa_y)\notin\mathcal{P}$, k_z is purely imaginary and the plane waves are evanescent. Eqn. (83) indicates that 3D Fourier-like integrals can be evaluated through 2D Fourier integrals, thus revealing that the EM field representation in the 3D space has two DoF. This is due to the Helmholtz's equation the field has to satisfy accounted for by $\widetilde{G}_0(\boldsymbol{\kappa})$ in (11). Moreover, it is worth noticing that for each condition in (85), the 2D integral includes only those plane waves propagating into the half-space that does not contain the source, as well as the evanescent waves. If $|\mathbf{r}| \gg \lambda$ and $\widetilde{\mathsf{A}}(\boldsymbol{\kappa})$ in (83) is slow varying around the value $\boldsymbol{\kappa}_\mathbf{r} = k_0\,\hat{\mathbf{r}}$, through the method of stationary phase, the following approximation holds [29, Ch. 12]

$$\begin{aligned}\int_{\mathcal{R}^2}\frac{\widetilde{\mathsf{A}}(\boldsymbol{\kappa})}{k_z(\kappa_x,\kappa_y)}\,e^{-\jmath\boldsymbol{\kappa}\cdot\mathbf{r}}\,d\kappa_x\,d\kappa_y &\simeq \widetilde{\mathsf{A}}(\boldsymbol{\kappa}_\mathbf{r})\int_{\mathcal{R}^2}\frac{e^{-\jmath\boldsymbol{\kappa}\cdot\mathbf{r}}}{k_z(\kappa_x,\kappa_y)}\,d\kappa_x\,d\kappa_y\\ &= \jmath 2\pi\widetilde{\mathsf{A}}(\boldsymbol{\kappa}_\mathbf{r})\frac{e^{-\jmath\,k_0\,|\mathbf{r}|}}{|\mathbf{r}|}\end{aligned} \tag{86}$$

where the last equality is known as Weyl's identity [32, Ch.1].

References

[1] M. Barbuto et al., "Metasurfaces 3.0: A new paradigm for enabling smart electromagnetic environments," *IEEE Trans. Antennas Propag.*, vol. 70, no. 10, pp. 8883–8897, Oct. 2022.

[2] D. Dardari and N. Decarli, "Holographic communication using intelligent surfaces," *IEEE Commun. Mag.*, vol. 59, no. 6, pp. 35–41, Jun. 2021.

[3] E. Björnson, H. Wymeersch, B. Matthiesen, P. Popovski, L. Sanguinetti, and E. de Carvalho, "Reconfigurable intelligent surfaces: A signal processing perspective with wireless applications," *IEEE Signal Process. Mag.*, vol. 39, no. 2, pp. 135–158, Mar. 2022.

[4] A. Abrardo, D. Dardari, and M. Di Renzo, "Intelligent reflecting surfaces: Sum-rate optimization based on statistical position information," *IEEE Trans. Commun.*, vol. 69, no. 10, pp. 7121–7136, Oct. 2021.

[5] K. Keykhosravi et al., "Leveraging RIS-enabled smart signal propagation for solving infeasible localization problems: Scenarios, key research directions, and open challenges," *IEEE Veh. Technol. Mag.*, vol. 18, no. 2, pp. 20–28, Jun. 2023.

[6] M. A. Jensen and J. W. Wallace, "Capacity of the continuous-space electromagnetic channel," *IEEE Trans. Antennas Propag.*, vol. 56, no. 2, pp. 524–531, Feb. 2008.

[7] D. A. B. Miller, "Waves, modes, communications, and optics: A tutorial," *Adv. Opt. Photon.*, vol. 11, no. 3, pp. 679–825, 2019. [Online]. Available: http://aop.osa.org/abstract.cfm?URI=aop-11-3-679

[8] H. Zhang et al., "Beam focusing for near-field multiuser MIMO communications," *IEEE Trans. Wireless Commun.*, vol. 21, no. 9, pp. 7476–7490, Sep. 2022.

[9] N. Decarli and D. Dardari, "Communication modes with large intelligent surfaces in the near field," *IEEE Access*, vol. 9, pp. 165648–165666, 2021.

[10] A. Díaz-Rubio and S. A. Tretyakov, "Macroscopic modeling of anomalously reflecting metasurfaces: Angular response and far-field scattering," *IEEE Trans. Antennas Propag.*, vol. 69, no. 10, pp. 6560–6571, Oct. 2021.

[11] Ö. Özdogan, E. Björnson, and E. G. Larsson, "Intelligent reflecting surfaces: Physics, propagation, and pathloss modeling," *IEEE Wireless Commun. Lett.*, vol. 9, no. 5, pp. 581–585, May 2020.

[12] D. Dardari, "Communicating with large intelligent surfaces: Fundamental limits and models," *IEEE J. Sel. Areas Commun.*, vol. 38, no. 11, pp. 2526–2537, Nov. 2020.

[13] S. A. Tretyakov, "Metasurfaces for general transformations of electromagnetic fields," *Phil. Trans. Roy. Soc. A, Math., Phys. Eng. Sci.*, vol. 373, no. 2049, Aug. 2015, Art. no. 20140362.

[14] K. Achouri, M. A. Salem, and C. Caloz, "General metasurface synthesis based on susceptibility tensors," *IEEE Trans. Antennas Propag.*, vol. 63, no. 7, pp. 2977–2991, Jul. 2015.

[15] V. Degli-Esposti, E. M. Vitucci, M. D. Renzo, and S. A. Tretyakov, "Reradiation and scattering from a reconfigurable intelligent surface: A general macroscopic model," *IEEE Trans. Antennas Propag.*, vol. 70, no. 10, pp. 8691–8706, Oct. 2022.

[16] V. S. Asadchy, M. Albooyeh, S. N. Tcvetkova, A. Díaz-Rubio, Y. Ra'di, and S. A. Tretyakov, "Perfect control of reflection and refraction using spatially dispersive metasurfaces," *Phys. Rev. B, Condens. Matter*, vol. 94, no. 7, Aug. 2016, Art. no. 075142, doi: 10.1103/PHYSREVB.94.075142.

[17] E. Martini and S. Maci, "Theory, analysis, and design of metasurfaces for smart radio environments," *Proc. IEEE*, vol. 110, no. 9, pp. 1227–1243, Sep. 2022.

[18] J. Zhu, Z. Wan, L. Dai, M. Debbah, and H. V. Poor, "Electromagnetic information theory: Fundamentals, modeling, applications, and open problems," *IEEE Wireless Commun.*, doi: 10.1109/MWC.019.2200602.

[19] G. Gradoni and M. Di Renzo, "End-to-end mutual coupling aware communication model for reconfigurable intelligent surfaces: An electromagnetic-compliant approach based on mutual impedances," *IEEE Wireless Commun. Lett.*, vol. 10, no. 5, pp. 938–942, May 2021.

[20] M. Najafi, V. Jamali, R. Schober, and H. V. Poor, "Physics-based modeling and scalable optimization of large intelligent reflecting surfaces," *IEEE Trans. Commun.*, vol. 69, no. 4, pp. 2673–2691, Apr. 2021.

[21] S. Droulias and A. Alexiou, "Reconfigurable intelligent surface: MIMO or radiating sheet?" *IEEE Trans. Wireless Commun.*, vol. 23, no. 4, pp. 2726–2739, Apr. 2024.

[22] M. Di Renzo, F. H. Danufane, and S. Tretyakov, "Communication models for reconfigurable intelligent surfaces: From surface electromagnetics to wireless networks optimization," *Proc. IEEE*, vol. 110, no. 9, pp. 1164–1209, Sep. 2022.

[23] A. S. Poon, R. W. Brodersen, and D. N. Tse, "Degrees of freedom in multiple-antenna channels: A signal space approach," *IEEE Trans. Inf. Theory*, vol. 51, no. 2, pp. 523–536, Feb. 2005.

[24] A. Pizzo, L. Sanguinetti, and T. L. Marzetta, "Fourier plane-wave series expansion for holographic MIMO communications," *IEEE Trans. Wireless Commun.*, vol. 21, no. 9, pp. 6890–6905, Sep. 2022.

[25] A. Pizzo, L. Sanguinetti, and T. L. Marzetta, "Spatial characterization of electromagnetic random channels," *IEEE Open J. Commun. Soc.*, vol. 3, pp. 847–866, 2022.

[26] A. Pizzo, A. Lozano, S. Rangan, and T. L. Marzetta, "Wide-aperture MIMO via reflection off a smooth surface," *IEEE Trans. Wireless Commun.*, vol. 22, no. 8, pp. 5229–5239, Aug. 2023.

[27] G. Oliveri, M. Salucci, and A. Massa, "Generalized analysis and unified design of EM skins," *IEEE Trans. Antennas Propag.*, vol. 71, no. 8, pp. 6579–6592, Aug. 2023.

[28] N. Shlezinger, G. C. Alexandropoulos, M. F. Imani, Y. C. Eldar, and D. R. Smith, "Dynamic metasurface antennas for 6G extreme massive MIMO communications," *IEEE Wireless Commun.*, vol. 28, no. 2, pp. 106–113, Apr. 2021.

[29] C. A. Balanis, *Antenna Theory: Analysis and Design*. Hoboken, NJ, USA: Wiley, 2016.

[30] R. F. Harrington, *Time-Harmonic Electromagnetic Fields*. New York, NY, USA: Wiley, 2001.

[31] X. Chen, *Computational Methods for Electromagnetic Inverse Scattering*. Hoboken, NJ, USA: Wiley, 2018.

[32] P. C. Clemmow, *The Plane Wave Spectrum Representation of Electromagnetic Fields*. Oxford, U.K.: Oxford Univ. Press, 1996.

[33] L. A. Zadeh, "Frequency analysis of variable networks," *Proc. IRE*, vol. 38, no. 3, pp. 291–299, Mar. 1950.

[34] M. T. Ivrlac and J. A. Nossek, "Toward a circuit theory of communication," *IEEE Trans. Circuits Syst. I, Reg. Papers*, vol. 57, no. 7, pp. 1663–1683, Jul. 2010.

[35] R. F. Harrington, "Matrix methods for field problems," *Proc. IEEE*, vol. 55, no. 2, pp. 136–149, Feb. 1967.

[36] S. Mason, "Feedback theory-further properties of signal flow graphs," *Proc. IRE*, vol. 44, no. 7, pp. 920–926, Jul. 1956.

[37] M. Berger, *Geometry I*. Berlin, Germany: Springer, 1987.

[38] G. A. E. Vandenbosch, "Reactive energies, impedance, and Q factor of radiating structures," *IEEE Trans. Antennas Propag.*, vol. 58, no. 4, pp. 1112–1127, Apr. 2010.

[39] S. Taravati and G. V. Eleftheriades, "Programmable nonreciprocal metaprism," *Sci. Rep.*, vol. 11, no. 1, p. 7377, 2021.

Davide Dardari (Senior Member, IEEE) is currently a Full Professor with the University of Bologna, Italy. He has been a Research Affiliate with Massachusetts Institute of Technology, USA. He has published more than 250 technical articles and played several important roles in various national and European projects. His research interests are in wireless communications, smart radio environments, localization techniques, and distributed signal processing. He received the IEEE Aerospace and Electronic Systems Society's M. Barry Carlton Award in 2011 and the IEEE Communications Society's Fred W. Ellersick Prize in 2012. He was the Chair of the Radio Communications Committee and a Distinguished Lecturer (2018–2019) of the IEEE Communications Society. He was also the Co-General Chair of the 2011 IEEE International Conference on Ultra-Wideband. He was also the TPC Chair of IEEE International Symposium on Personal, Indoor and Mobile Radio Communications (PIMRC 2018), the TPC Co-Chair of the Wireless Communications Symposium of the 2007/2017 IEEE International Conference on Communications, and TPC Co-Chair of the 2006 IEEE International Conference on Ultra-Wideband. Currently, he is a Senior Member of the Editorial Board of *IEEE Signal Processing Magazine*. He served as an Editor for IEEE TRANSACTIONS ON WIRELESS COMMUNICATIONS from 2006 to 2012 and as a guest editor for several journals.

Open Access funding provided by 'Alma Mater Studiorum - Università di Bologna' within the CRUI CARE Agreement